

043
SVB
13474L

MEASUREMENT OF ELECTRON-ATOM SCATTERING CROSS SECTIONS
AT LOW ENERGIES BY PHOTOELECTRON SPECTROSCOPY

by

K.P. SUBRAMANIAN

A THESIS
SUBMITTED FOR THE DEGREE OF

DOCTOR OF PHILOSOPHY

OF THE
GUJARAT UNIVERSITY

043



B13474

AUGUST 1987

PHYSICAL RESEARCH LABORATORY

AHMEDABAD 380 009

INDIA

എന്റെ അമ്മേ അപ്പാ

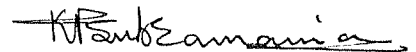
To

My Parents

PHYSIOLOGICAL RESEARCH LABORATORY
LIBRARY
Cl. No. 043 Date. 9/12/77
SUB
Acc No. 13474 Price, 6

C E R T I F I C A T E

I hereby declare that the work presented in this thesis is original and has not formed the basis for the award of any degree or diploma by any University or Institution.



K.P. Subramanian

Certified by:



Vijay Kumar
Ahmedabad.

August, 1987

STATEMENT

The basic aim of the work presented in this thesis is to measure the electron scattering cross-sections for noble atoms at low electron energies. In this energy region, new theoretical models for calculating the electron-atom scattering cross-section accurately are now available in literature with the result that a direct comparison of the experimental data is now possible. Experimentally, low energy electron scattering studies are difficult and somewhat challenging. Not much data are available in this electron energy region. An experiment has been designed and fabricated in the laboratory to measure absolute total electron-atom scattering cross-sections using a photoelectron source. This is the first time when such a study has been carried out using the powerful technique of photoelectron spectroscopy. The electron scattering cross-sections have been carried out for helium, neon, argon, krypton and xenon at seventeen electron energies ranging from 0.7 to 10 eV with an accuracy of $\pm 2.7\%$.

Basic experimental set-up consists of a monochromatic VUV photon source, beam-splitter, photoionising/scattering cell, electron energy analyser, electron detector and data acquisition system. VUV photons from strong emission lines are allowed to interact with source gas kept at low

pressure inside the ionising region. Noble gas atoms (argon, krypton and xenon) are used as source gas for the production of photoelectrons. Photoionisation of source gas leads to the production of electrons with two energies, corresponding to $^2P_{1/2}$ and $^2P_{3/2}$ state of the ion thus produced. Using various combinations of photon energies and source gases, seventeen energy points could be generated in the electron energy region ranging from 0.7 to 10 eV. Photoelectrons thus produced are allowed to undergo scattering in the cell where target gas is introduced. The photoelectrons are then energy analysed and the intensities of photoelectron peaks are monitored as a function of target gas pressure. Sometimes source and target gas are one and the same. Total scattering cross-sections are derived from these observations. The experimental set-up has been described in detail in chapter 2 of the thesis whereas the subject of electron scattering at low energies has been introduced in chapter 1.

An analytical method has been developed to compute the scattering cross-sections from the observations for attenuations of photoelectron peaks due to the introduction of target gas in the scattering region. Two methods for data analysis have been developed when source and target atoms are the same and when these are different. These methods have been discussed in chapter 3 of the thesis.

The major errors taken into account are errors from

pressure measurement, thermal transpiration effects, scattering in the accelerating region of the energy analyser, uncertainty in the scattering path length, counting statistics, forward scattering of electrons, gas impurities etc. Coherent sum of all these errors acted as upper limit to the actual error and it came out to be $\pm 5.3\%$. The incoherent sum of all these errors represent the most probable error which is $\pm 2.7\%$ in this experiment. All errors and their estimated magnitudes have been discussed in detail in chapter 4 of the thesis.

The total electron scattering cross-sections for helium as measured in the present experiment are comparable with those reported by other investigators using transmission techniques and time-of-flight measurements and using variational methods to express helium ground-state wave function. The electron-neon scattering cross-sections also compare well with the measurements made other investigators and theoretical calculations using adiabatic exchange approximations and R-matrix theory. In the case of argon, the scattering cross-sections reported in the present work compare well those measured by transmission techniques but disagree in some limited energy regions with measurements obtained by time-of-flight technique. There is a good agreement between our results and those reported by R-matrix calculations. Electron scattering cross-sections for krypton and xenon obtained in the present work at electron energies upto 5 eV compare well with the values

given by other investigators using transmission technique but at higher energies, there is a discrepancy between different set of experimental data. Unfortunately, at electron energies above 2 eV, the results reported using different theoretical models for both krypton and xenon disagree to a large extent with the results obtained by different experimental techniques. The results for the present experiment have been discussed in detail in chapter 5 of the thesis whereas conclusion and scope for future work has been taken up in chapter 6.

ACKNOWLEDGEMENTS

I take this opportunity to thank my Ph.D. Supervisor Prof. Vijay Kumar for the encouragement and enthusiastic support throughout the period of my doctoral work. He has been always a great source of inspiration throughout my Ph.D. career. I express my sincere gratitude to him for his affection, and also for critically going through the manuscript of the thesis and making several useful suggestions.

I thank Prof. V.B. Sheorey for his help and encouragement. I have had many fruitful discussions with him on the theoretical aspects of scattering physics. I would like to thank Professors B.H. Subbaraya and A.C. Das for having taken keen interest in my progress.

I owe a lot to my senior colleagues and friends Drs. E. Krishnakumar and Ajai Kumar. I have had a lot of discussions with them at every stage of the work. My thanks are also due to my friend Mr. Maqbool Ahmed who has been a nice company in and outside the laboratory.

Our group members have rendered a lot of help for my Ph.D. work. I am extremely thankful to Mr. A.P. Gohil for helping with the data acquisition system. Helps rendered by Messrs I.T. Kripalani and J.K. Dave in developing and upkeeping relevant electronics equipments are invaluable. Messrs I.A. Prajapati and R.S. Patel had helped in instrumentation and Mr. V.K. Lodha was always offering a helping hand in maintaining the vacuum system. I thank them sincerely.

My thanks are due to Messrs H.N. Chandel and M.N. Trivedi for their help in the construction of experimental system. I thank the staff of workshop, glass-blowing section, liquid-nitrogen plant, drafting section, photographic section and also the staff of library and computer centre for various helps during the course of my work.

I would like to thank my friends Vijay Sankar, Vinod, Bhaskaran, Krishna Kumar, Raju, Mathew, Debi, Sunil, Janardhan and Banerjee, whose company I enjoyed a lot during my stay in PRL.

This thesis was prepared on DEC-1091 computer with the help of word processing software developed by Dr. B.R. Sitaram and Mr. Amarendra Narain. My thanks are due to them. I sincerely thank Mr. Philip C. Samuel for his

assistance in storing the manuscript in the computer files
and for editing and processing it neatly.

Finally, I thank all my friends and well wishers who
have directly and indirectly helped me in completing this
work successfully.

(K.P. Subramanian)

Ahmedabad

August, 1987

CONTENTS

CERTIFICATE

STATEMENT

ACKNOWLEDGEMENT

CHAPTER ONE : INTRODUCTION

1.1	Scattering cross-section	1
1.2	Different types of electron collisions	2
1.2.1	Elastic collisions	3
1.2.2	Inelastic collisions	4
1.2.3	Superelastic collisions	4
1.2.4	Radiative collisions	5
1.3	Total scattering cross-section	5
1.3.1	Relationship of Q with observables	6
1.4	Applications of electron scattering studies	7
1.4.1	Application to atmospheric physics and astrophysics	8
1.4.2	Application to gaseous dielectrics and laser physics	10
1.4	Survey of theoretical methods for cross-section calculations	12
1.5.1	Potential scattering - method of partial waves	14
1.5.2	Close-coupling approximation	15
1.5.3	R-matrix theory	17

1.5.4	Method of polarised orbitals	19
1.5.5	Variational methods	21
1.6	Survey of experimental methods	23
1.6.1	Ramsauer's method	24
1.6.2	Linearised Ramsauer method	27
1.6.3	Time-of-flight method	28
1.6.4	Swarm experiments	30
1.7	Comparison of energy resolution of electrons in scattering experiments	33
1.7.1	Advantages of using photoelectron source over other sources	35
1.8	Measurement of scattering cross-section using a photoelectron source	38

CHAPTER TWO : EXPERIMENTAL SET-UP

2.1	Introduction	40
2.2	Photoelectron source	41
2.2.1	VUV Light source	43
2.2.2	Beam monitor	46
2.2.3	Ionising region	48
2.2.4	Electron energies available	48
2.3	Scattering of photoelectrons	49
2.4	Energy analysis of photoelectrons	51
2.4.1	Choice of energy analyser	52
2.4.2	Cylindrical Mirror Analyser - design aspects	56
2.4.3	Analyser details	59
2.4.4	Accelerating/retarding region	60
2.4.5	Magnetic field shielding	61
2.4.6	Effects of contact potentials	62

2.5	Electron detector	63
2.5.1	Choice of detector	64
2.5.2	Perfomance of detector	66
2.6	Vacuum chamber	67
2.6.1	Design of vacuum system	69
2.7	Pressure measurement	70
2.8	Data acquisition system	72
2.9	Operation of the photoelectron spectrometer	74
2.9.1	Perfomance of the spectrometer	77
2.10	Scattering by target atoms	77
2.10.1	When source and target gases are different	78
2.10.2	When source and target gases are same	78

CHAPTER THREE : METHOD FOR CALCULATION OF SCATTERING CROSS-SECTION

3.1	When source and target gases are different	83
3.2	When source and target gases are same	87

CHAPTER FOUR : ERROR ANALYSIS

4.1	Pressure measurement	91
4.1.1	Instrument calibration	91
4.1.2	Reference pressure	93
4.2	Thermal transpiration	93
4.3	Uncertainty in scattering path length	94
4.4	Counting statistics	95
4.5	Forward scattering	97
4.6	Multiple scattering	98
4.7	Scattering in the accelerating region	99

4.8	Gas impurity	100
4.9	Scattering due to ions	100
4.10	Uncertainty in incident electron energy	101

CHAPTER FIVE : RESULTS AND DISCUSSIONS

5.1	Helium	103
5.2	Neon	105
5.3	Argon	106
5.4	Krypton	108
5.5	Xenon	110

CHAPTER SIX : CONCLUSION AND SCOPE FOR FUTURE WORK

6.1	Conclusion	113
6.2	Scope for future work	115

LIST OF PUBLICATIONS

REFERENCES

CHAPTER ONE

INTRODUCTION

1.1 Scattering cross-section

When a collimated beam of projectile particles is incident on a group of localized target particles (scatterers), the incident beam is scattered into different solid angles by the scatterers. The assumptions made to model this problem are the following:

1. The current density, J_0 , of the incident particles is small such that the interaction among the individual particles in the beam could be ignored.
2. The momenta of the incoming particles are sufficiently low such that the de Broglie wave lengths associated

with them are small as compared to the distance between the scattering centres. In other words, coherent effects due to multiscatterers could be neglected in a single scattering event.

Schematic diagram of scattering is given in figure 1.1. Number of particles scattered, dN , into a solid angle $d\Omega$ is proportional to the number of scatterers, n , current density of the incident particles, I_0 , and $d\Omega$. Or,

$$dN = \sigma(\theta, \phi) n I_0 d\Omega$$

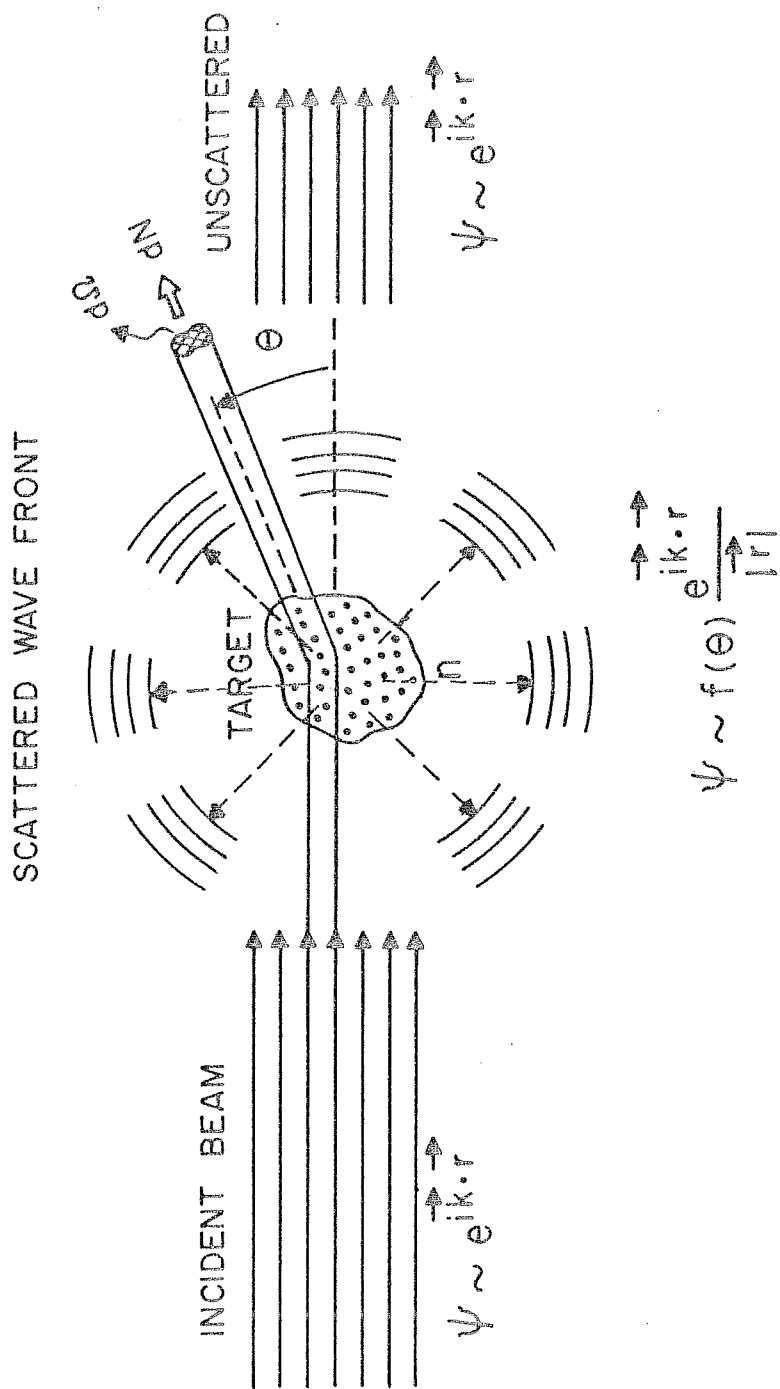
where σ is known as the scattering cross-section. Obviously, σ depends on k , the energy of the particles in the incident beam and is a function of solid angle variables θ and ϕ . For a spherically symmetric potential, σ does not depend on the azimuthal angle, and in such cases $\sigma(\theta, \phi) = \sigma(\theta)$. Dimension of scattering cross-section is area, and physically it is interpreted as the cross-sectional area of the scatterer contributing to the scattering event.

1.2 Different types of electron collisions

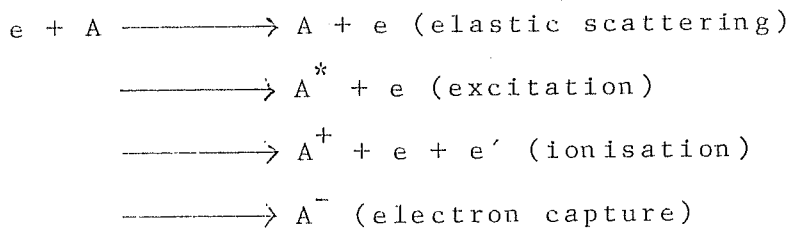
We restrict ourselves to electron-atom or electron-molecule collisions. Different kinds of collisional phenomena can occur, depending upon the energy of the electron beam as well as the nature of the target species.



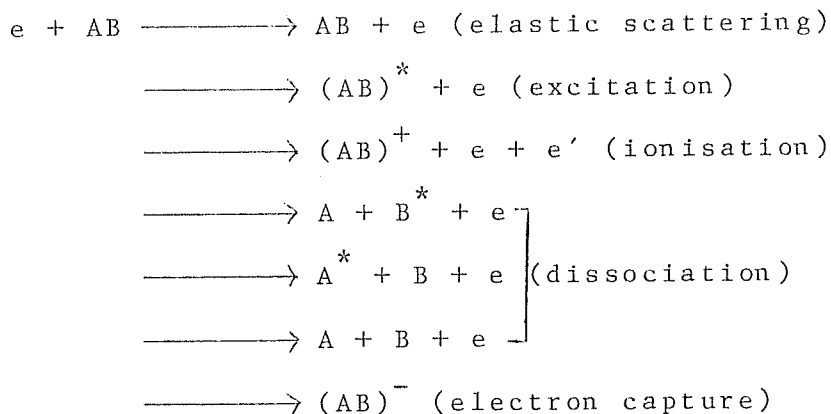
Fig.1.1 SCHEMATIC DIAGRAM OF SCATTERING



where i and j represent the initial and final state of the scatterer, A. For atomic targets, these include



and for molecules



A cross-section σ_{ij} could be attached to each of the channels given above. Further classification of scattering cross-section is given below:

1.2.1 Elastic collisions

When internal state of the projectile or target particle does not change during the collision, it is referred to as elastic collision. In other words, σ_{ii} is called elastic scattering cross-section. However, in elastic collisions, energy transfer among the scattering bodies is possible through exchange of momentum. Though energy is conserved in centre of mass co-ordinate of the system, transfer of velocity is possible to the centre of mass. A

fraction of energy of the order $\frac{m}{M}$ is lost by the projectile particle in the process of collision, m and M being masses of projectile and target species respectively. For elastic scattering of electrons with atoms or molecules, this fraction is of the order of 10^{-3} and could safely be neglected.

1.2.2 Inelastic collisions

In inelastic collisions, the energy in the centre of mass of the colliding system is not conserved due to internal excitation of incident or target particles. Thus σ_{ij} , where $i \neq j$ correspond to inelastic scattering cross-section. Further classification of inelastic cross-section is done depending upon the channel of reaction during collisional process. These are rotational, vibrational and electronic excitation cross-section etc.

1.2.3 Superelastic collisions

In this case target is already in the excited state and during collision, the projectile particle gains energy from the scatterer. This often happens when electrons collide with atoms in metastable state. Energy is transferred to the centre of mass of the system from the internal motions of the atoms.

1.2.4 Radiative collisions

This is similar to superelastic collision, but instead of transferring energy to electron, atom in metastable state de-excites by emitting a quantum of radiation. Even though energy is conserved in the centre of mass, this type of collision is regarded as inelastic because of the change in internal configuration of the atom. Sometimes while emitting the radiation, the energy loss suffered by the target atom is large enough to trap the incident electron and form a negative ion.

1.3 Total scattering cross-section

The quantity $\sigma(\theta, \phi)$ discussed above is called differential scattering cross-section, and it varies at different angles with respect to the incident electron beam direction. Differential scattering cross-section integrated over all solid angles is known as total scattering cross-section, Q_{ij} . Total scattering cross-section is also classified in terms of different channels such as total elastic scattering cross-section, total ionisation cross-section etc.

$$Q_{ij} = \int \sigma(\theta, \phi) d\Omega$$

All these cross-sections summed over all possible channels, including $i \rightarrow i$ (i.e. elastic), is known as total scattering cross-section, Q .

$$Q = \sum_{i,j} Q_{ij}$$

In general, various units are used to represent scattering cross-sections and these have been reviewed by Bederson and Keiffer [1971]. Normally, cross-sections are expressed in cm^2 . At times, they are presented in terms of P_c , the number of collisions suffered by an electron during 1 cm travel at 1 Torr of pressure at 0°C . This could be converted to cm^2 by $\sigma = 2.83 \times 10^{-17} P_c$. σ is also used frequently in terms of a_0 , the first Bohr radius.

$$\begin{aligned} \sigma(\text{cm}^2) &= \sigma(\pi a_0^2) \times 0.880 \times 10^{-16} \\ &= \sigma(a_0^2) \times 0.283 \times 10^{-16} \end{aligned}$$

1.3.1 Relationship of Q with observables

Total scattering cross-section, Q , as measured in transmission experiments, is derived from the attenuation of the projectile beam after its passage through the scattering medium. In the case of measurement of total electron scattering cross-section, a well collimated electron beam of initial intensity I_0 is passed through the scattering medium inside a scattering cell. The attenuation of beam intensity after passage through scattering medium is related to the number density, n , of the target atoms present in the cell, the path length travelled in the medium, x , and the total scattering cross-section, Q , of the target gas species. The attenuated beam intensity is given by

$$I = I_0 \exp(-nQx)$$

This is known as Beer-Lambert law.

Electrons once scattered are deviated from the primary beam and will not contribute to the beam again. The assumption here is that the electrons during its transit time are scattered only once. To ensure this, the target gas pressure in the scattering cell has to be maintained at a low value, such that the mean free path of electron at that pressure is larger than the path length of electrons in the scattering cell, x .

1.4 Applications of electron scattering studies

Scattering cross-section studies have found applications in almost all branches of physics. Historically, this was one of the areas which has contributed immensely to the development of quantum mechanics and many body problems. Theoretical study of collisional phenomena, even today is an active field of research. As a result, new models and techniques are available to give better insight of physics of collisions. Since the advent of fast supercomputers and new algorithms, the research leading to numerical evaluation of cross-sections also has flourished, yielding more accurate data.

Other areas which greatly depend upon some aspects of collision physics are astrophysics, atmospheric physics,

plasma research and applied physics which include gaseous dielectrics, laser physics etc.

1.4.1 Applications to atmospheric physics and astrophysics

There are large number of applications of electron collisions with atoms and molecules in both atmospheric and astrophysics. It is almost impossible to enumerate and discuss all these applications. Only a few of these would be taken up and discussed briefly.

In gaseous nebulae, electrons are produced by the interaction of stellar u.v. radiation with the major constituents of the nebulae like hydrogen, helium and traces of other elements. Typical values of electron density in gaseous nebulae are 10^3 to 10^4 cm^{-3} and average electron temperature, T_e is of the order of 10^4 K [Osterbrock, 1974]. Electron-electron collisions, which are much faster than electron-atom collisions are mainly responsible for setting up of the Maxwellian distribution of electrons. However, free electrons contribute to collisional excitation of low lying metastable states of the ion. One such process leads to the formation of the metastable state $O^{++}(^1D)$ through electron collisions. Through inelastic collisions, the $O^{++}(^1D)$ gets de-excited to $O^{++}(^3P)$ state followed by radiative emission of lines corresponding to wavelengths 4959 and 5007 Å [Seaton, 1968]. These correspond to the green "nebulium" lines first observed by Higgins in 1864.

In earth's atmosphere, the production mechanism of electrons is photoionisation of gases by solar u.v. radiation. To start with, these electrons possess a broad range of energies. As electrons cool down through collisions, they cause excitation of neutral particles, and are populated in metastable states. De-excitation of these states is followed by the radiative emission. This results in the illumination of sky, known as day-glow. Intensities of day-glow for some line emissions have been computed by Wallace and McElroy [1966], Green and Barth [1967] and Dalgarno [1968]. Allen [1982] has given a detailed account of emission lines important to astrophysics as well as atmospheric physics.

In the earth's ionosphere, the electron gas is heated by elastic collisions with photoelectrons and superelastic collisions with metastable species. Because of high efficiency of energy transfer in collisions of one electron with another, a Maxwellian distribution for velocity is rapidly established, characterized by a temperature T_e which will tend to be greater than neutral particle temperature T_n . The heated electron gas cools by a variety of collision processes. One of the best ways for electron cooling is the energy transfer of electrons in inelastic collisions with heavy particles leading to electron-neutral scattering. The total energy transfer rates in the upper atmosphere depend

upon the number density of electrons, electron and neutral temperatures and cooling rates for different neutral constituents of the atmosphere. All these cooling rates require electron scattering cross-sections and number densities of the neutrals.

1.4.2 Applications to gaseous dielectrics and laser physics

The study of electron collisions with certain molecules has applications in a special branch of physics known as gaseous dielectrics. In this field, knowledge of electron attachment (electron affinity) leading to the formation of negative ions, slowing down of electrons through collisional processes, and electron impact ionisation of molecular gases is required to choose gases inside the devices like circuit breakers, high voltage research equipments, transformers etc.

It can be seen that in a gas (number density, N) subjected to an applied electric field E , the free electrons attain an equilibrium energy distribution $f(\epsilon, E/N)$ which is a function of the gas and E/N [Christophorou et al, 1984]. For low value of E/N , the number of electrons having sufficient energy to ionise the gas is negligible and hence the gas is an insulator. When applied electric field is increased, $f(\epsilon, E/N)$ shifts to higher energy region liberating electrons with sufficient energy to ionise the gas, and the gas becomes a conductor. This phenomenon is known as electrical breakdown in gases.

The most efficient way to prevent electrons from initiating breakdown is to remove them by attachment to the gas molecules forming stable negative ions. Due to increase in inertia, negative ions show slow response to applied electric fields. Thus electron attachment cross-sections at various energies has to be known for the proper choice of the gas inside these devices. Role of buffer gas is also important in gaseous dielectrics. The buffer gas maximises the efficiency of electron attachment of gas by scattering them into an electron energy region in which the electronegative gas attaches them efficiently.

Collision physics has found vast application in the field of lasers. Since the discovery of lasing action in gases (He-Ne), a large number of lasing atoms and molecules have been identified so far. This has resulted in the development of neutral atomic lasers, ionic lasers and molecular lasers.

In order to obtain stimulated radiation from a gaseous medium, a necessary (but not sufficient) condition is that population inversion takes place when the upper-laser-state density (divided by its statistical weight) is greater than the lower-laser-state density (divided by its statistical weight). The laser radiation takes place when the stimulated radiation is greater than the combined losses in the

gaseous medium. These losses include diffusion of the excited molecules to the walls, collisional and radiative decay of the excited species, absorption in gas and transmission losses through the mirrors and windows. The common methods adopted to excite the gas medium in the laser are gas discharge, electron beam and electron beam assisted gas discharge. Thus scattering cross-section data in selective excitation channels become very relevant in laser physics. Several reviews are available in literature, in which the role of collision physics in the operation of various lasers has been discussed in detail [Phelps, 1974, 1979; Bekefi, 1976; Cherrington, 1979; Rhodes, 1979; McDaniel and Nighan, 1982 and Christophorou, 1984].

1.5 Survey of theoretical methods for cross-section calculations

There are quite a few theoretical methods available in literature for the calculation of electron scattering cross-section for atoms at low electron energies. A few of these methods would be discussed in this section briefly.

At this point, it is necessary to define low energy scattering explicitly. In electron scattering with atoms, the complete energy domain may be divided into three regions, viz. low, intermediate and high energy regions. Though there is no clear demarkation between these regions, the classification is done in accordance with the physical

considerations like the open channels involved in the process, electron residence time in the vicinity of target atom etc. Another procedure of classifying collision process is based on comparing the velocities of incident electrons (free electrons) to the velocities of bound electrons in the target atom. This will decide the extent of correlation effects to be incorporated in the model potential. Normally upto a couple of tens of eV energy of incident electrons, it is considered as low energy scattering, a few tens to a few hundreds intermediate and above it, it is considered as high energy scattering. For low energy collisions, exchange and correlation effects are important, and these inclusions make the calculation of cross-section complicated.

Scattering cross-sections are generally computed from the phase shift of the wave function of the incident electron. In low energy scattering, partial wave analysis gives a direct relation between the phase-shift and cross-section. For the sake of completeness, method of partial waves would be described briefly. Other methods discussed in this section for the calculation of cross-section are close-coupling approximation, R-matrix theory, polarized orbital method and lastly variational methods. A detailed account of various theoretical methods for scattering problems are given by Callaway [1980]. A brief discription of various theoretical techniques is given by Sheorey [1976]. These techniques would be discussed briefly, and their usefullness under different conditions would be

pointed out wherever possible.

1.5.1 Potential scattering - method of partial waves

The wave front of the incoming projectile particles is represented by plane waves and the scattered wave front by spherical waves modulated by probability amplitude, $f_k(\theta)$

$$e^{i\mathbf{k} \cdot \mathbf{r}} \longrightarrow f_k(\theta) \frac{e^{i\mathbf{k} \cdot \mathbf{r}}}{r} + e^{i\mathbf{K} \cdot \mathbf{r}} \quad (1.4)$$

In the case of potential scattering, angular momentum is a conserved quantity. Therefore, if we analyse the incoming plane waves in terms of spherical waves with quantized angular momentum, the effect of scattering would be an introduction of phase-shift in the radial part of the wave function. Decomposition of plane waves in terms of spherical partial waves is achieved by a unitary transformation in Hilbert space. It could be seen that, the radial part of the wave functions are spherical Bessel functions and angular parts are Legendre polynomials. For plane wave advancing in z-direction,

$$e^{ikr \cos \theta} = \sum_{\ell=0}^{\infty} (2\ell+1) i^{\ell} F_{\ell}(kr) P_{\ell}(\cos \theta) \quad (1.5)$$

For $r \rightarrow \infty$, the Bessel functions have the asymptotic form $\sin(kr - \frac{1\pi}{2})$, and after scattering, due to the introduction of phase shift,

$$F_{\ell}(kr) \sim \sin(kr - \frac{1\pi}{2} + \delta_{\ell})$$

Probability amplitude can be derived as

$$f_k(\theta) = (2ik)^{-1} \sum_{\ell=0}^{\infty} (2\ell+1) (e^{2i\delta_{\ell}} - 1) P_{\ell}(\cos \theta) \quad (1.6)$$

and scattering cross-section

$$Q = \frac{4}{k^2} \sum_{l=0}^{\infty} (2l+1) \sin^2 \delta_l \quad (1.7)$$

Thus it is clear that phase shifts completely determine scattering cross-section. For low energy scattering, only few partial waves are to be included, as the contribution from higher order terms turns out to be insignificant. This theory has successfully explained many early observations in collision physics, such as cross-section minima of noble gases with higher mass number at low energies, which is popularly known as Ramsauer-Townsend effect.

1.5.2 Close-coupling approximation

There is a close connection between the electron plus target atom/ion collision problem and the problem of calculating bound state wave functions of neutral atoms or positive ions. In this approximation, only a few atomic eigenstates in the expansion for the total wave function of $(N+1)$ electrons are retained.

For a target atom with nuclear charge Z and number of electrons N , the nonrelativistic Hamiltonian is

$$\hat{H}(Z, N) = -\sum_{i=1}^N (\nabla_i^2 + \frac{2Z}{r_i}) + \sum_{i,j} \frac{2}{r_{ij}} \quad (1.8)$$

$Z > N$ refers to positive ions, $Z = N$ for neutral and $Z < N$ denotes negative ions.

The Schrodinger equation for such a bound system is

$$\hat{H}(Z, N) \psi_i = E_i(Z, N) \psi_i(1, 2, \dots, N) \quad (1.9)$$

which gives infinite number of bound states converging to

nearest ionisation limit, $E_{\infty}(Z, N)$. For $E > E_{\infty}$ we have one electron in the continuum and a positive ion core with $(N-1)$ electrons. This is identical to scattering of the electron in the continuum with a $(N-1)$ electron target atom.

The Hamiltonian for scattering with N electron target atom could be written as

$$\hat{H}(Z, N+1) = -\sum_{i=1}^{N+1} (\nabla_i^2 + \frac{2Z}{r_i}) + \sum_{(i,j)} \frac{2}{r_{ij}} \quad \text{--- (1.10)}$$

and the Schrodinger equation is

$$\hat{H}(Z, N+1) \Psi(N+1) = E \Psi(1, 2, \dots, N+1) \quad \text{--- (1.11)}$$

To solve for Ψ , Ψ is expressed in terms of the core wave function ψ and free electron wave function $F_i(r_{N+1})$ summed over all open channels and a few closed channels of the target atom.

$$\Psi(N+1) = \mathcal{A} \sum \psi_i(1, 2, \dots, N) F_i(r_{N+1}) \quad \text{--- (1.12)}$$

where \mathcal{A} antisymmetrises total wave function in space and spin co-ordinates. The total wave function is expressed as a linear combination of core and free electron wave functions.

Applying variational principle

$$\langle \Psi | H - E | \Psi \rangle = 0 \quad \text{--- (1.13)}$$

a set of coupled integro-differential equations are obtained for the radial wave function $F(r)$ and its coefficients. In their review article on numerical solution of such integro-differential equations, Burke and Seaton [1971] have given the details of the radial equations and of the numerical methods employed to solve them.

This approximation describes well the strong

transitions between low lying states, well separated from energy, from all other states and is one of the best method for low energy scattering studies. However, efficiency with which a particular problem is done depends on the number of terms in the eigen function expansion and the proper choice of correlation function.

1.5.3 R-matrix theory

The R-matrix theory was originally developed for application in nuclear physics [Wigner, 1946; Wigner and Eisenbud, 1947] and later on has found tremendous application in atomic collision theory. In this method, the configuration space for the $(N+1)$ electron-atom system is divided into two regions: an inner region, $0 < r < a$, where electron correlations are strong and difficult to treat and an outer region, $a < r < \infty$ where the final state wave function is usually analytically solvable. In the inner regions, the wave functions are slowly varying functions of energy. These two regions are investigated using different theoretical approaches and the wave functions are matched on the surface of the sphere of radius 'a'. Electron exchange is important in the inner region, whereas it could be neglected in the outer region. The boundary radius a is chosen to be large enough such that all ionic core functions are effectively zero for $r > a$. In outer regions, the collisions are described by coupled differential equations (rather than integro-differential equations), which often have

analytical solution, or at least a solution achievable by numerical techniques [LeDourneuf et al, 1977].

The wave function as well as its derivatives are matched at the boundary $r = a$, or in other words, if the wave function is to satisfy the boundary condition,

$$\frac{a}{u(r)} \frac{du}{dr} = b \quad \text{-----} \quad (1.14)$$

where $u(r)$ is the radial wave function describing the motion of electrons and b is an arbitrary constant which may depend on the channel quantum number. The R-matrix is defined in terms of the logarithmic derivative of radial wave function on the surface of the inner region.

R-matrix theory yielded good results for low mass number atoms in low energy regions. Extension of this technique is possible to non-spherical and multicentre scatterers such as molecules [Shneider, 1977]. Recently, R-matrix theory has been applied for positron scattering studies in hydrogen and nitrogen molecules [Tennyson, 1986]. Algorithms and computer codings for numerical calculations using this technique are published by Berrington et al [1974, 1978]. However, there are discrepancies in the results obtained using this method in atoms with larger mass-number, especially towards higher energy ($\sim 10\text{eV}$). It is possibly due to the complexities in the inner region.

1.5.4 Method of polarized orbitals

A theoretical description of low energy electron-atom collision must make allowance for electron exchange and for the distortion of the target atomic electron wave functions. The polarized orbital method originally proposed by Temkin and Lamkin [1961] incorporates both these aspects. A brief account of this method is given below, where specific application of this method to electron-hydrogen atom collision is described. Recently, method of polarized orbitals has been applied to many electron atomic systems such as neon [Dasgupta and Bhatia, 1984; McEachran and Stauffer, 1985].

The total wave function $\Psi(r_1, r_2)$ for electron-hydrogen scattering system may be written as

$$\Psi^{\pm}(r_1, r_2) = (1 + \hat{P}_{12}) [\phi_0(r_1) + \chi(r_1, r_2) F^{\pm}(r_2)] \quad (1.15)$$

where \hat{P}_{12} is the exchange operator of electrons 1(atomic) and 2(incident). The sign \pm shows singlet or triplet state of wave functions and $F(r)$, ϕ_0 and F are target atom and incident electron wave functions and χ represents the change in the hydrogen atom wave function when it is perturbed by the presence of the incident electron fixed at r_2 ($r_2 > r_1$). The approximation here is that the velocity of incident electron is much less than orbital velocity of the target atomic electron. Therefore, the atomic electron gets sufficient time to readjust itself in the presence of the

field of incident electron, or the process is adiabatic.

could be reduced to first order equation as

$$\begin{aligned} \chi(r_1, r_2) &= - \epsilon(r_1, r_2) \frac{P_\ell(\cos \theta_{12})}{\sqrt{\pi}} \\ \text{where } \epsilon(r_1, r_2) &= 1, \quad r_2 > r_1 \\ &= 0, \quad r_2 < r_1 \\ \text{and } \cos \theta_{12} &= \frac{r_1 \cdot r_2}{r_1 r_2} \end{aligned} \quad (1.16)$$

Using variational principle

$$\delta \int \Psi^* (H - E) \Psi \, d^3r_1 \, d^3r_2 = 0$$

one obtains the integro-differential equation for the scattered wave function

$$\begin{aligned} \left[\frac{d^2}{dr^2} - \frac{\ell(\ell+1)}{r^2} - u(r) + \frac{\mathcal{L}(r)}{r^4} + k^2 \right] F_\ell(r) \\ = \int K_\ell(r, r') + K_\ell^P(r, r') F_\ell(r') \, dr' \end{aligned} \quad (1.17)$$

Here \mathcal{L} represent long range static polarization potential.

Also, there are additional non-local terms represented by kernel K_1^P (dynamic polarization) and exchange term represented by K_1 . The approximation in which the dynamic polarization part K_1^P is neglected is known as exchange adiabatic approximation.

The polarized orbital method has been extended to include full perturbation due to the distortion of atomic target. Thus quadrupole terms are also included in the long range part of the potential. Allowance for non-adiabaticity by inclusion of terms arising from first order correction due to finite velocity of incident electron also has been made. The results obtained by this method compare well with the results from other methods, especially in low energy

region.

1.5.5. Variational methods

An important theoretical technique, which is regarded as being the most accurate available for the calculation of low energy elastic scattering, is the variational method. For example, the S-wave phaseshifts calculated for electron-hydrogen scattering by Schwartz [1961] using a variational method are considered as the most accurate available, even today. A brief account of the variational method for elastic scattering by a potential $u(r)$ which satisfies the boundary conditions

$$\left. \begin{aligned} \lim_{r \rightarrow 0} r u(r) &= -2Z \\ \text{and } \lim_{r \rightarrow \infty} r u(r) &= 0 \end{aligned} \right\} \dots \dots \dots (1.18)$$

(Z being the nuclear charge), is given below.

The radial Schrodinger equation for the problem is

$$\begin{aligned} \mathcal{L} F &= 0 \\ \text{where } \mathcal{L} &= \frac{d^2}{dr^2} - \frac{l(l+1)}{r^2} - u(r) + k^2 \end{aligned} \quad \left. \dots \dots \dots (1.19) \right\}$$

The solutions $F_l(kr)$ satisfies the boundary conditions

$$\begin{aligned} F_l(0) &= 0 \\ \text{and } \lim_{r \rightarrow \infty} F_l(kr) &= k^{-1/2} \left[\sin \left(kr - \frac{l\pi}{2} \right) + \tan \delta_l(k) \cos \left(kr - \frac{l\pi}{2} \right) \right] \end{aligned} \quad \left. \dots \dots \dots (1.20) \right\}$$

where $\tan \delta_l(k)$ is the scattering phaseshift.

Consider a trial solution F^t , not necessarily the solution of $\mathcal{L} F = 0$, but satisfying the boundary conditions

$$\begin{aligned} F^t(0) &= 0 \\ \text{and } \lim_{r \rightarrow \infty} F_l^t(kr) &\sim \sin \left(kr - \frac{l\pi}{2} \right) + A^t \cos \left(kr - \frac{l\pi}{2} \right) \end{aligned} \quad \left. \dots \dots \dots (1.21) \right\}$$

For such a wave function it can be shown that

$$\delta \left[\langle F^t | \mathcal{L} | F^t \rangle + A^t \right] = 0 \quad \dots \dots \dots (1.22)$$

It may be pointed out here that addition of arbitrary wave functions to F^t , which vanishes at the boundaries $r = 0$ and ∞ does not alter the variational condition (1.22). Thus the short-range effects such as electron exchange and/or electron correlations may be allowed for by adding such functions (i.e. which vanish at both boundaries) to the trial function.

There are different procedures to obtain the scattering phaseshift, A^t . The Kohn phaseshift [Kohn, 1948] is given by

$$\tan \delta_\ell^K = \tan \delta_\ell^t - \langle F^t | \mathcal{L} | F^t \rangle \quad (1.23)$$

Further details about variational methods are discussed by Demkov [1958] and Moiseiwitsch [1966].

The matrix variational method, which is essentially a generalization of the Kohn variational method to multichannel problems, has been used to accurately calculate low energy electron scattering by complex atomic targets. This work has been largely done by Nesbet and his collaborators. The method has been reviewed by Nesbet [1980] and Callaway [1978].

Accurate s-wave and p-wave phaseshifts have been calculated by Nesbet [1979] for low energy elastic scattering of electrons by helium. For higher partial waves, the Born approximation was employed. The calculated

cross-sections for energy below 19 eV were estimated to be within 1% of the exact results, and this serves as a calibration standard for other theoretical techniques as well as for experiments. A detailed comparison of these and other theoretical methods with our observations will be presented in chapter 5.

1.6 Survey of experimental methods

Experimental methods for the measurement of electron scattering cross-section could be broadly divided into two groups. These are transmission experiments and swarm techniques. The approach of these two methods is entirely different. In Ramsauer type of experiments, an electron beam, after proper energy selection, is transmitted through the scattering medium and quantities like number of electrons scattered into different solid angles, attenuation of electron beam etc. are measured as a function of electron energy. Scattering cross-sections are directly deduced from such observations. On the other hand, in swarm technique, effect of applied electric and magnetic field on the passage of electrons through a medium is studied, and macroscopic transport properties are measured. Cross-sections are derived from such measurements.

A third method is that of crossed-beams which is substantially different from the other two. In this method, incident as well as target particles are prepared in the

form of beams and are crossed mutually. Interaction region is defined by the crossed volume. Particles scattered into various angles with respect to either of the beam direction, transmitted intensity of incident beam etc. are measured in these experiments. One obvious advantage of this method over the others is that this offers possibility to undertake scattering experiments on target particles prepared in selective states such as excited states, ionic state etc. Also, spin aligned studies of either projectile or target particles, scattering by transient species etc. are possible using this method.

Some of the transmission methods like Ramsauer method, linearised Ramsauer method and time-of-flight technique have been described briefly in this section. In some of the sophisticated transmission type of experiments, the target particles are prepared in the form of beam to cross it with the interacting electron beam. Such methods have not been described separately but while discussing various transmission methods, mention has been made, wherever possible, when the projectile and target particles are used in the form of beams. A brief description of the swarm experiments has also been made in the section.

1.6.1 Ramsauer's method

Ramsauer's method is the pioneering effort to measure electron scattering cross-section quantitatively. Originally

developed to study the energy distribution of electrons from metals due to the interaction of u.v. radiation, this method was later extended to measure electron scattering cross-sections in gases. The schematic diagram of the experiment used by Ramsauer and his co-workers [Ramsauer, 1921] is shown in figure 1.2.a.

Metal photoelectrons were ejected from zinc cathode C by irradiating it with a mercury arc light source. The ejected electrons were confined in a spiral orbit by applying an external magnetic field, B , perpendicular to the plane of the diagram. Region E, where slits s_1 to s_5 are arranged on the circumference of a circle discriminates energy of the electrons admitted into the scattering region. S is the scattering region. Electrons scattered inside the cell S go to the wall, and S records scattered current I_s , while A records direct anode current I_a . The magnetic field has two-fold advantages; firstly, it assists in energy-selection, and secondly, it provides remarkable energy resolution through momentum discrimination of elastically and inelastically scattered electrons (except for elastically forward scattered electrons).

At pressures p_1 and p_2 in the apparatus, if I_{s1} and I_{s2} and I_{a1} and I_{a2} are the currents detected by S and A, then

$$I_{s1} = (I_{s1} + I_{a1}) e^{-\lambda p_1 x}$$

$$I_{s2} = (I_{s2} + I_{a2}) e^{-\lambda p_2 x}$$

$$\text{or } \frac{I_{s1}}{I_{s2}} = \frac{(I_{s1} + I_{a1})}{(I_{s2} + I_{a2})} e^{-\lambda (p_1 - p_2) x}$$

Fig. 1.2a RAMSAUER'S METHOD

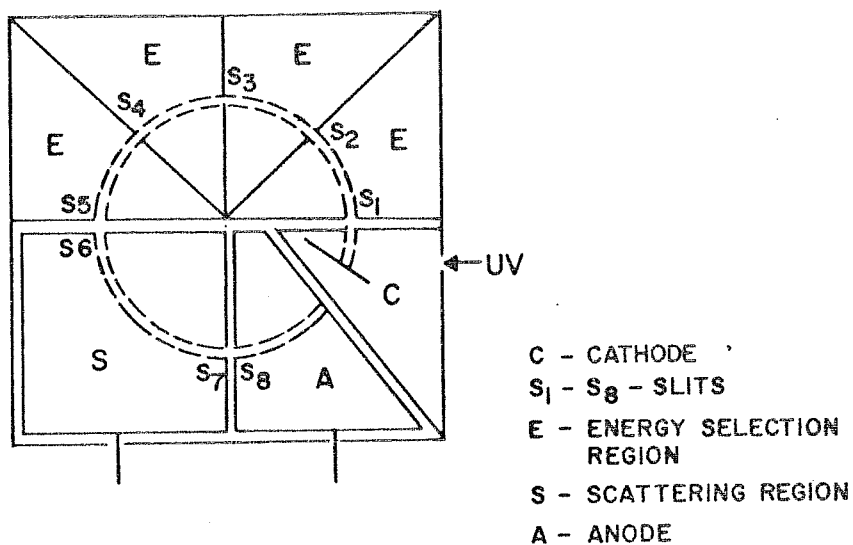
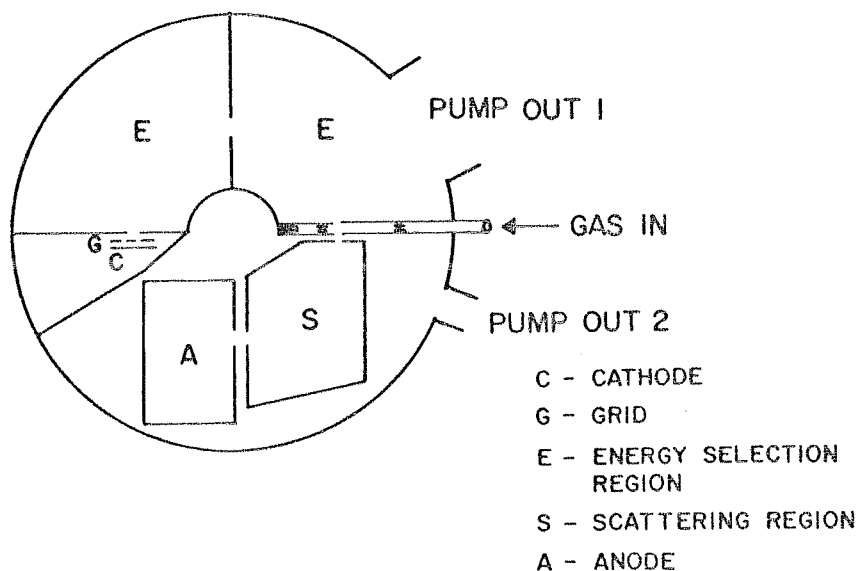


FIGURE 1.2.b. MODIFIED RAMSAUER METHOD
 (GOLDEN AND BANDEL (1965))



where λ is a parameter directly related to cross-section and x is the distance between slits S_6 to S_7 along the electron trajectory.

In spite of the limitations of the experiment, like presence of scattering gas in energy selection and electron production regions, this experiment provided good results. Later on these limitations were taken care of by Ramsauer and Kollath [1929] and Rusch [1925]. Using this technique, they were able to establish low energy cross-section minima for heavy noble gases (Ar, Kr and Xe), postulated by Townsend and Bailey using swarm measurements in argon [1921, 1922a, 1922b, 1923]. This phenomenon is popularly known as "Ramsauer-Townsend effect".

The Ramsauer method was improvised and perfected by several investigators in this field. Notables among them were Brode [1925], Normand [1930], Bruche et al [1927] and later on by Golden and Bandel [1965]. Brode's apparatus could be operated at elevated temperatures ($\sim 400^\circ\text{C}$) and this rendered study of cross-section in some metal vapours possible. Other modifications were improved electron sources, introduction of the concept of differential pumping and more reliable techniques for absolute pressure measurements. Schematic diagram of the modified Ramsauer apparatus used by Golden and Bandel [1965] is shown in figure 1.2.b. The whole apparatus was machined from a single block of metal and coated with colloidal graphite to minimize the problem

of contact potentials. Thermionic electrons with pre-acceleration grids were used, thereby rendering more electron energies accessible. The electron production and analysing regions were differentially pumped using two separate pumps; thus scattering of electrons in the analysing region was minimized. Finally the pressure measurements inside the scattering cell were accomplished by a Shultz-Phelps ionisation gauge calibrated against a standard gauge. These improvements made the observed data more accurate and reliable. Recently Dalba et al [1979] have used a similar kind of apparatus for the measurement of scattering cross-section in helium, with a modified scattering cell geometry, so as to minimize detection of multi-scattered electrons from the cell.

1.6.2 Linearised Ramsauer method

In this class of experiments, instead of using magnetic field for energy selection a pre-monochromatised electron beam is passed through a linear scattering cell, where electron scattering takes place. Major improvements achieved in using this method are improved electron optics, studies of scattering at different angles and post-scattering energy analysis of electron beam. Present-day linearised devices have the capabilities of measuring temperature as well as temperature and pressure gradients in the scattering cell. Data provided by these experiments are precise and free from systematic errors. Stein et al [1978]

using a beam transmission technique measured electron-atom scattering cross-sections for helium and neon at low electron energies. The same experimental set-up was used for positron-atom scattering, by replacing the electron source with a positron source and the requisite optics [Kaupilla et al, 1977]. A large number of other investigators have also used linearised Ramsauer technique; a few amongst them are Nickel et al [1985] and Blaauw et al [1977, 1980] who measured electron scattering cross-sections for helium, neon, argon and xenon for electron energies greater than 4 eV and for helium for electron energies greater than 15 eV respectively.

1.6.3 Time-of-flight methods

One of the recent advances in the electron scattering studies is the advent of time-of flight scattering spectroscopy. There is an ever increasing demand for the high resolution electron beam scattering experiments to test various theories, especially in the low energy region. Also, to study phenomena like resonances in scattering, high resolution experiments are indispensable. Time-of-flight scattering experiments supercede earlier ones in energy resolution, especially at low electron energies.

Another obvious advantage of time-of-flight spectroscopy is that, the electron energies are sharply defined. In electron monochromators, electron energies for

scattering studies are obtained by tuning electric or magnetic fields, thus invoking high degree of uncertainty in energy. In other words, the energy of electrons supplied by the monochromator is dictated by passive variables like voltages on deflecting plates or current in magnetic coil. On the other hand, in the time-of-flight technique, the electron energy is derived by accurately measuring the time taken by the electron to travel across the flight length, L . Thus energy is derived directly from parameters which are fundamental by nature.

In a time-of-flight spectrometer, the electrons before entering the scattering cell are chopped by a chopper wheel at a repetition frequency, $f_{\text{gate}} = \frac{1}{T}$, where T is the period (first time-mark). In some spectrometers, bunches of electrons are produced from metal surfaces by irradiating it with pulsed u.v. source. These electrons proceed towards the detector and arrive at different times depending upon their energy. Another synchronous gate (second time-mark) enables the detector for detecting electrons for a specified time interval. To avoid frame overlap, one has to ensure that the beam gate period T , is larger than the longest particle flight time t_{max} . This process is cyclic and hence this method is a pulsed experiment. This makes the signal level very low, and this is one of the drawbacks of this type of experiment. Scattering studies are done by introducing gas into the scattering cell. Scattering cross-sections are calculated by monitoring reduction in

intensity of the electron beam.

Detailed review for this technique is provided by Raith [1976]. Using this method, Ferch et al [1980] and Jones [1985] have measured scattering cross-section for molecular hydrogen. Ferch et al [1985b] have used this technique to investigate Ramsauer minimum in methane. Land and Raith [1974] have measured resonances in oxygen molecule scattering cross-section, while Charlton et al [1980], Kennerly and Bonham [1978] and Ferch et al [1985a] have measured scattering cross-sections for argon and helium, for helium and for argon respectively.

1.6.4 Swarm experiments

In swarm experiments, the scattering cross-section is worked out from the macroscopic observables, viz. the transport coefficients of a gas. These kinds of experiments are particularly useful in measuring mean energy loss suffered by slow electrons with gas atoms or molecules. This type of cross-section is termed as momentum transfer cross-section.

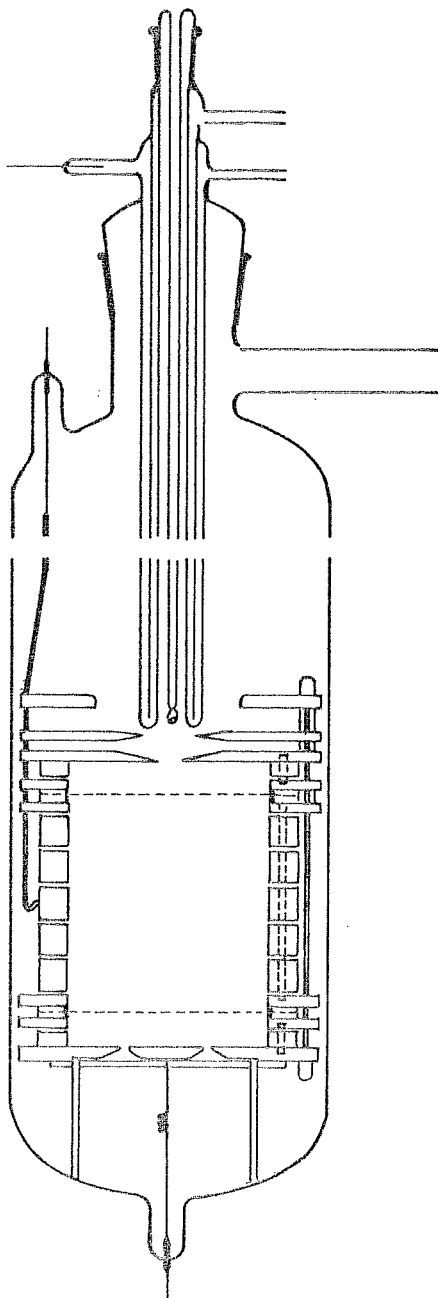
In swarm experiments, transport parameters of an electron beam under the influence of electric and magnetic fields are measured. Electron densities are controlled to be sufficiently low so that space-charge effects can be neglected. The observables are:

1. The electron drift velocity, $W_{||}$ along a uniform electric field, E ,
2. The ratio of $\frac{D_{\perp}}{\mu}$, where D_{\perp} is the diffusion coefficient perpendicular to the electric field and μ is the mobility.
3. The ratio of $\frac{W_{||}}{W_{\perp}}$ where W_{\perp} is the electron drift velocity at right angles to crossed uniform electric and magnetic fields.

The cross-sections are related to transport coefficients through collision terms in the Boltzmann equation. In his review article, Allis [1956] has summarized the application of first order perturbation theory to the solution of binary Boltzmann collision integral, in the presence of a weak electric field.

The schematic diagram of a drift tube is shown in figure 1.3.a [Crompton et al, 1965]. $W_{||}$ is measured from direct time-of-flight measurements. $\frac{D_{\perp}}{\mu}$ is obtained using Townsend-Huxley method which consists of measuring the ratio of total current traversing a region of uniform magnetic field to a fraction of current which has drifted off due to collision. $\frac{W_{||}}{W_{\perp}}$ is measured by observing the asymmetry in current collected by the splitted anode A (figure 1.3.b) caused by $E \times B$ drift. These observables are related to momentum transfer cross-section σ_{MT} and the

Fig. 1-3 a SCHEMATIC DIAGRAM OF A DRIFT TUBE
SWARM EXPERIMENT
(CROMPTON et al 1967)



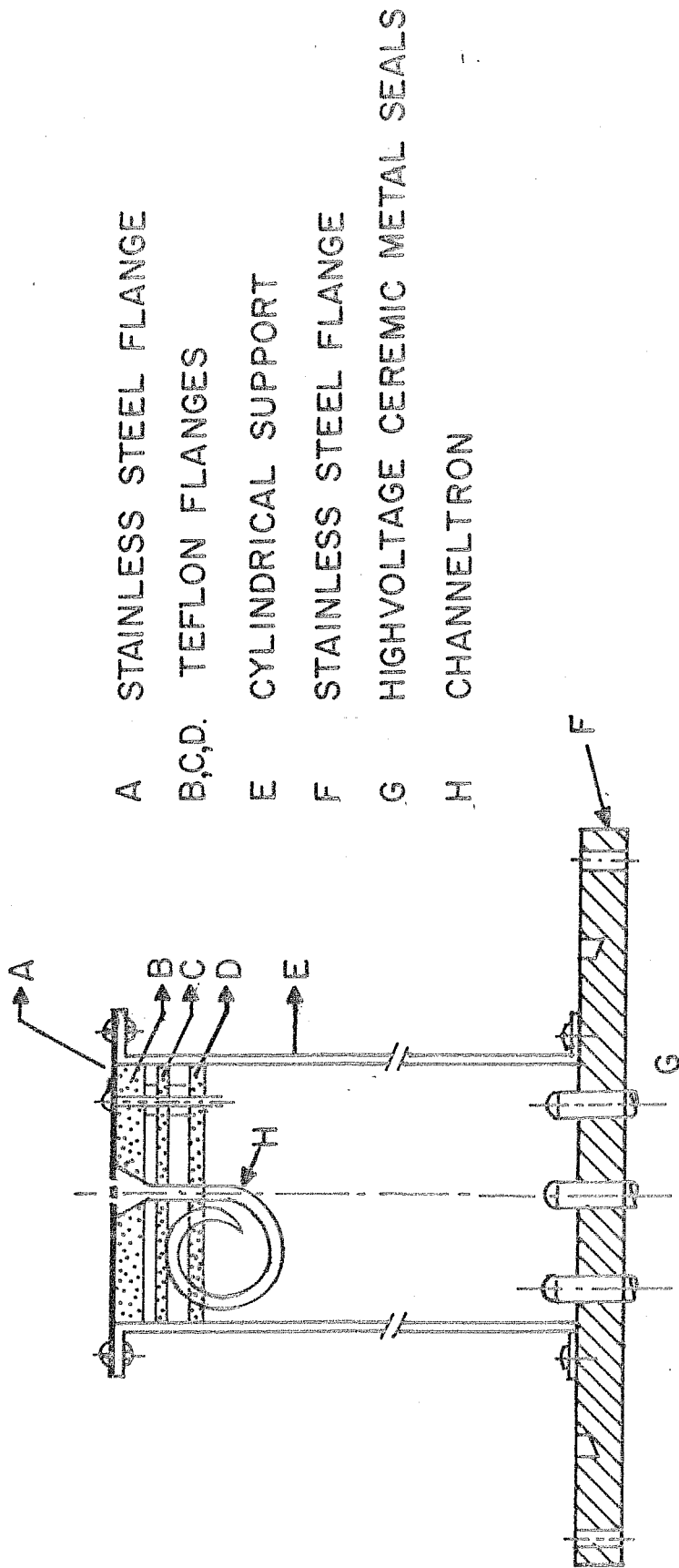


Fig. 2.5 SCHEMATIC DIAGRAM OF CHANNELTRON HOUSING

Table 2.3 Characteristics of Mullard CEM-B419BL
Channeltron

1. Maximum operating voltage	: 3.5 kV
2. Normal resistance	: 5×10^9 ohm
3. Gain (@ 2.5 kV)	: 1.1×10^8
4. Noise (@ 2.5 kV)	: 2.0 p.p.s
5. Pulse height distribution distribution (@ 10^8 gain and 1000 p.p.s)	: 0.6
6. Maximum effective cone diameter	: 9 mm

Note : The observed noise was about 1 count per
10 sec.

a comparator.

The output end circuit alongwith a ripple filter circuit for the +3 KV power supply were housed near the channeltron in the vacuum system. The negative pulses developed at the rear end of the channeltron were capacitively coupled to a high input impedance charged sensitive preamplifier, whose fall time was fixed around 1μ sec. The preamplifier output was further amplified through a capacitively coupled amplifier, whose gain was adjusted in such a way that the variable threshold discriminator cut off noise and gave clean TTL compatible pulses.

2.6 Vacuum chamber

The vacuum chamber which houses the complete experiment to measure the electron scattering cross-section is shown in figure 2.6. It consists of three stainless steel chambers of almost the same size.

The photoelectron spectrometer was housed in the middle chamber, which was 45.7 cm long and 35.6 cm in diameter (18 and 14 inches, nominal). The inner and the outer cylinders of the CMA were mounted on a $3/4$ inch thick stainless steel flange which separated the first from the middle chamber. In other words, this flange separated the beam splitting region and analysing region.

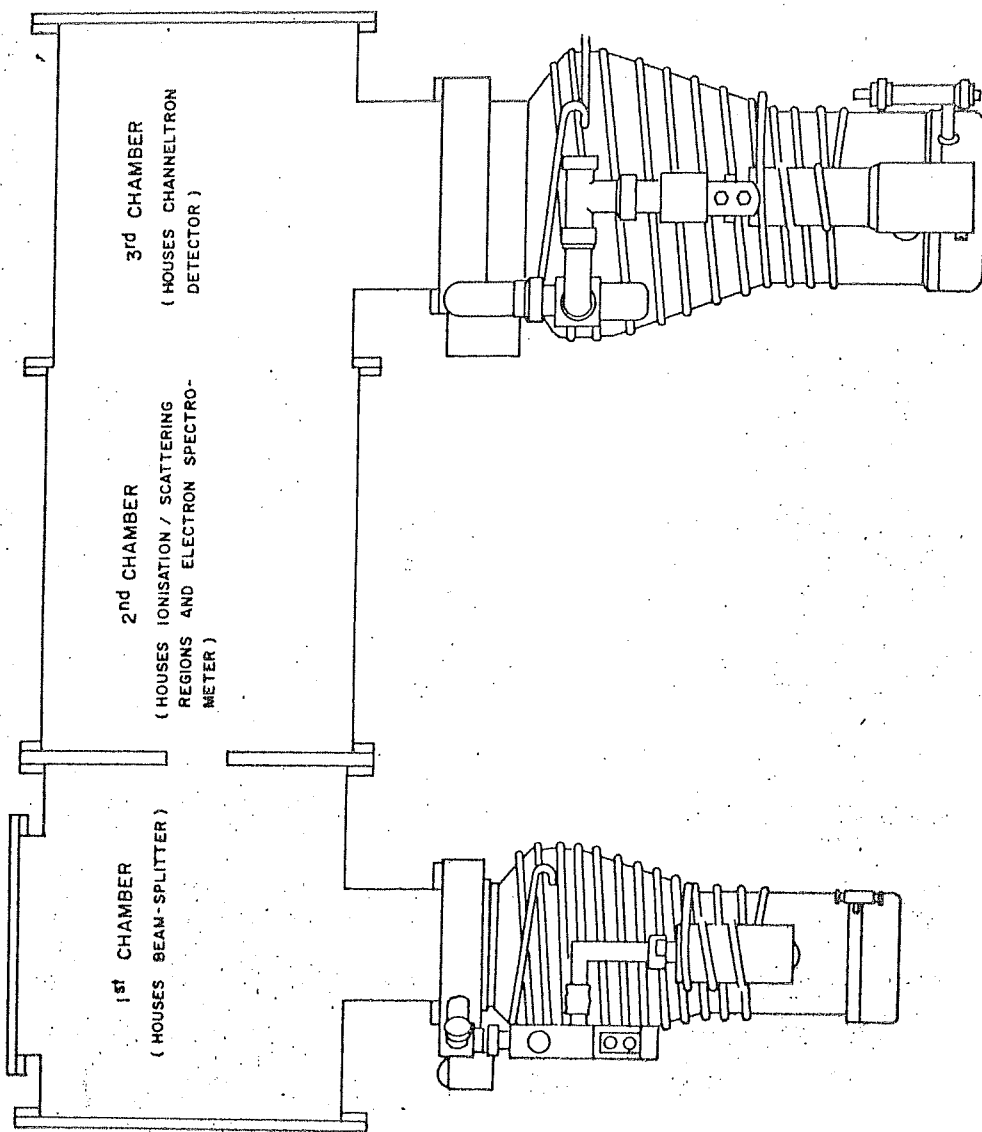


FIG.2.2.6 VACUUM CHAMBER

The first chamber which was in between the light source and photoelectron spectrometer was 40.6 cm long and 35.6 cm in diameter (16 and 14 inches, nominal) and housed beam splitter assembly. This chamber was evacuated by a diffstak pump [Edwards MK2 160/700P] with a pumping speed of 700 lit./sec. and backed by a two stage rotary pump [Edwards EDM 20A]. The diffstak pump was connected to a 15.2 cm (6 inch) diameter side arm on the chamber. A 25.4 cm (10 inch) diameter port was provided diametrically opposite to the diffstak pump to have easy access to the inner parts of the system. Two ceramic feed-throughs were also provided in this chamber for electrical connections to the inner electrode of the spectrometer. Other ports available on this chamber were one for photomultiplier housing (beam splitter) and two each for gas introduction and absolute pressure measurement in the system. The accelerating region was connected to the beam splitter region with practically no impedance in between and therefore this line acted as the first stage of the differential pumping for the analysing region.

The third chamber was 40.6 cm (16 inch) long and 33 cm (13 inch) in diameter. This housed the detector system, and was connected to the middle chamber through a rotatable flange. A 25.4 cm (10 inch) diameter side port was provided on which a diffstak pump [Edwards MK2 250/2000P] was mounted, backed by a two stage rotary pump [Edwards E 2M 40]. This diffstak pump pumps the analysing as well as the

detecting region and acted as the second stage of the differential pumping.

2.6.1 Design of vacuum system

Various parts in the vacuum system were designed, so as to obtain various dynamic differential pressures in different parts of the system. This was achieved by computing conductances of the differential pumping lines along with the pumping speeds and matching these with the throughputs.

Using different formulae for conductances [Dushman, 1962; Guthrie, 1963] of various pumping lines of different geometry and conductances of slits and apertures the pumping speed for the two diffstak pumps to be used with the system were calculated. This was done when the ultimate vacuum of 10^{-6} Torr was required with no source and target gas in the ionising region and 5×10^{-5} Torr when source/target gas was present in the ionising region with 50μ of pressure ($1 \mu = 10^{-3}$ Torr). For a known pressure of gas in the ionising region, the pressures in the accelerating and analysing regions were computed by comparing throughputs of gas. In the viscous flow region, the formula itself contained the average pressure of the conducting line. In such cases, the pressure was calculated iteratively, until calculated values of pressure were self-consistent.

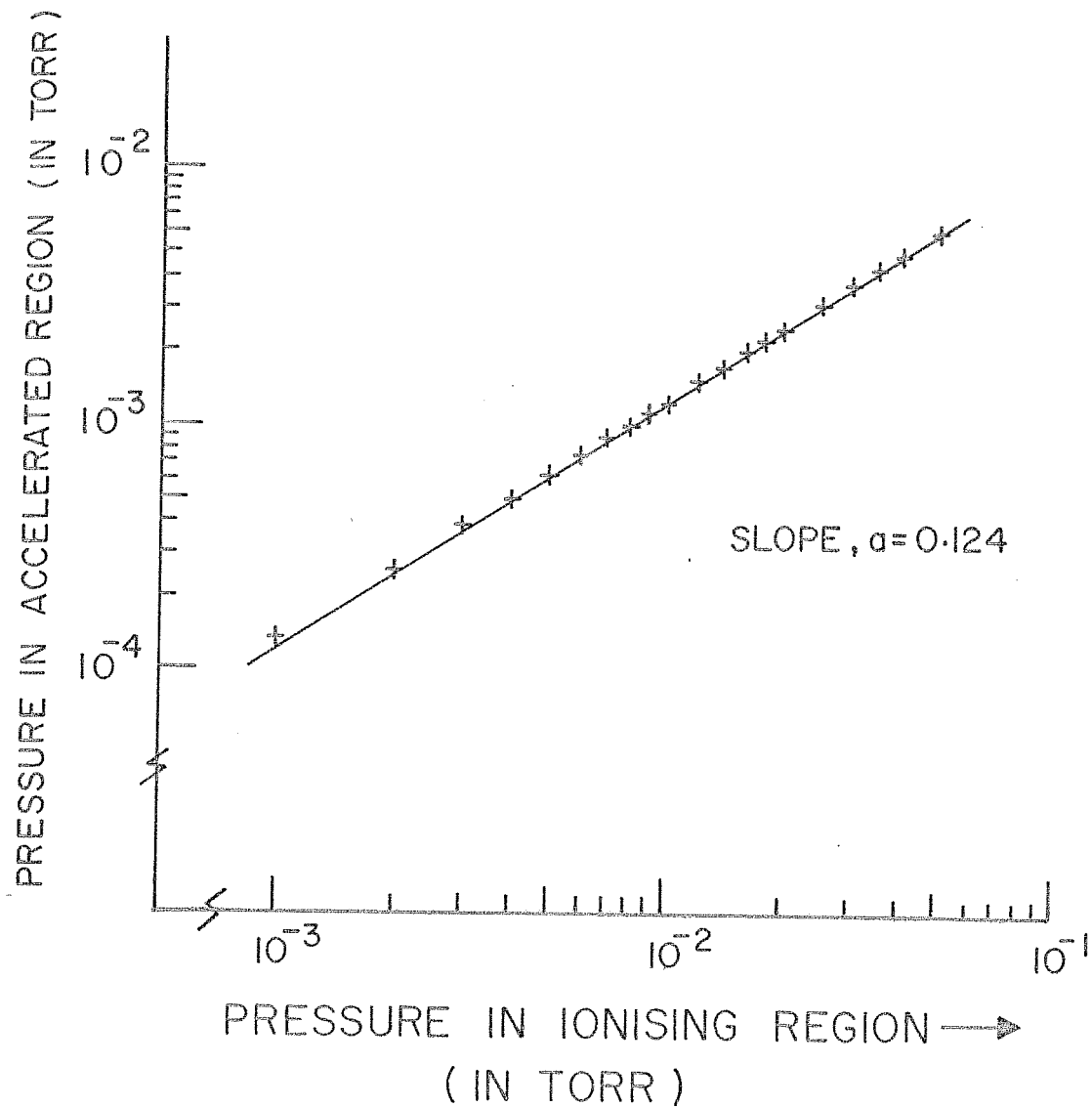
The vacuum system has been designed in such a way as to have a pressure difference 15 to 20 times less in the accelerating region and 200 to 250 times less in the analysing region as compared to pressures in the ionising region which could vary from 1 to 50 microns. A comparison of pressures in the ionising and accelerating regions for helium pressures ranging from 1 to 50 micron in the ionising region is shown in figure 2.7. It has to be pointed out that, both these pressures were measured absolutely. Also, it has to be noted that the pressure in the accelerating region was measured at a point immediately above the slit. Therefore, it may show slightly higher pressure than the average pressure in the accelerating region.

2.7 Pressure Measurement

A variety of vacuum gauges were used in the present experiment. These were thermocouple gauge, penning gauge, ionisation gauge and MKS Baratron capacitance manometer. Each of these had different functions and served different purposes.

All other gauges, except MKS Baratron, were not absolute gauges and these were used to estimate the order of vacuum at different parts of the experimental chamber. The measurement of pressure by these gauges depends on one or

Fig. 2.7 RATIO OF PRESSURES IN IONISING
AND ACCELERATING REGIONS



other property of the gas used, and hence are non-standard. Thus, the measured vacuum, using these gauges tended to vary from gas to gas under identical physical conditions. Therefore for measuring absolute pressure, these gauges have to be calibrated for each sample gas used in the experiment, which is very tedious.

The pressures in the ionisation/scattering region had to be measured absolutely and accurately. This was solely because the number density of target particles in this region was required to compute electron scattering cross-sections. This was derived from the pressure measured absolutely. A calibrated MKS capacitance manometer was used for this purpose (MKS Instrument, BH 1). This was a differential gauge and therefore the reference side of the gauge had to be evacuated by an oil diffusion pump. Sensitivity of this gauge was 10^{-6} Torr, provided the reference side was evacuated to 10^{-7} or 10^{-8} Torr. Since in the present work pressures strating from 10^{-4} to 10^{-2} Torr had to be measured, the reference side was maintained at around 10^{-6} Torr.

The same gauge head was used to determine the absolute pressures in the ionising as well as accelerating region. The connection diagram of the MKS Baratron is shown schematically in figure 2.8. A, B, and C were greaseless shut-off valves made of glass (Kontes, N.J.). To start with valves A and B were closed and balancing valve C was open.

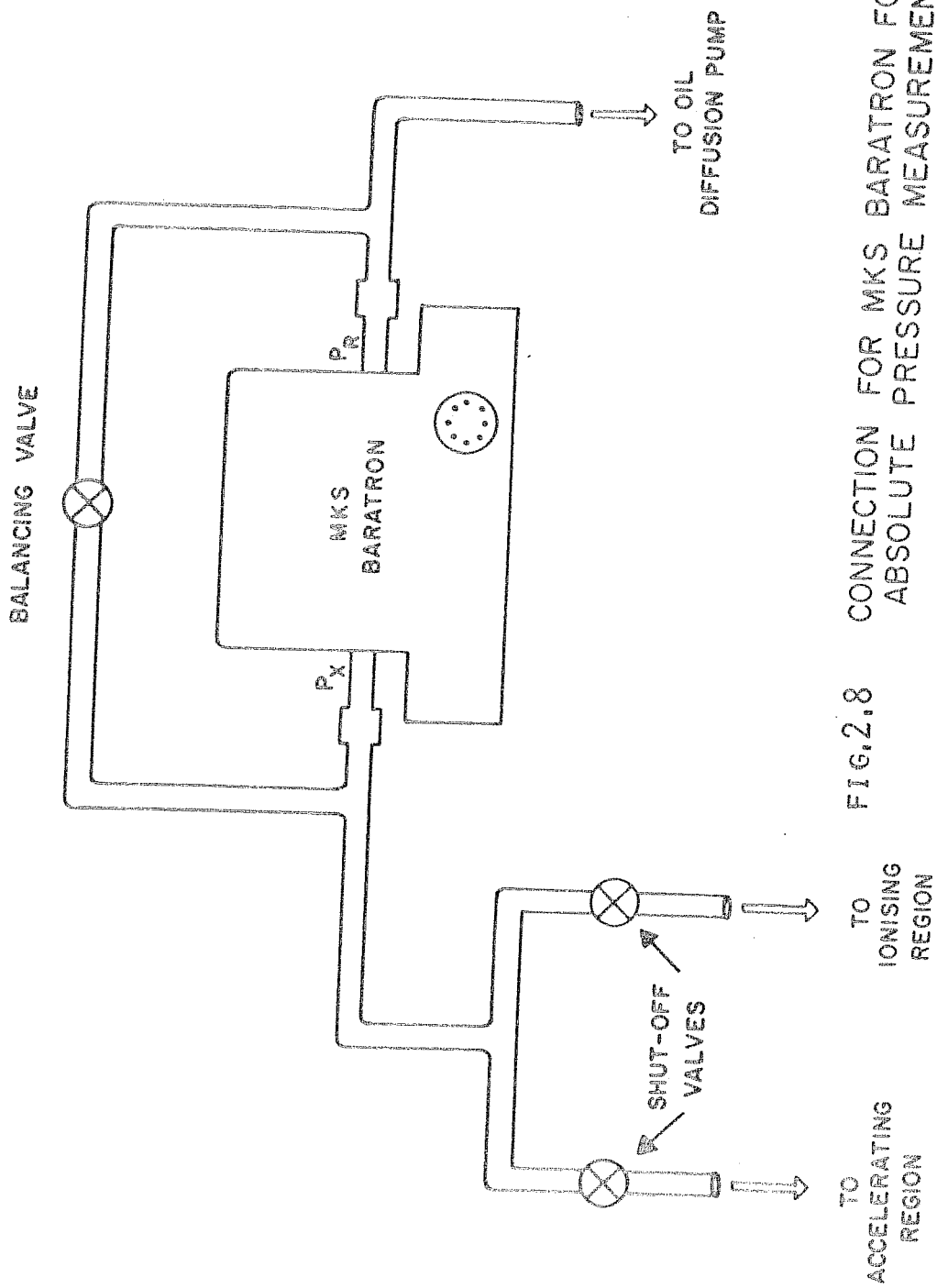


FIG.2.8 CONNECTION FOR MKS BARATRON FOR ABSOLUTE PRESSURE MEASUREMENT

Both sides of the Baratron were brought to a vacuum of 10^{-6} Torr, and adjustments were done in the meter so as to obtain null reading in the read-out unit in the most sensitive range of the meter. The meter is set to be balanced now. Balancing valve C was closed, and absolute pressure either in ionising or scattering region was measured by opening valve A or B.

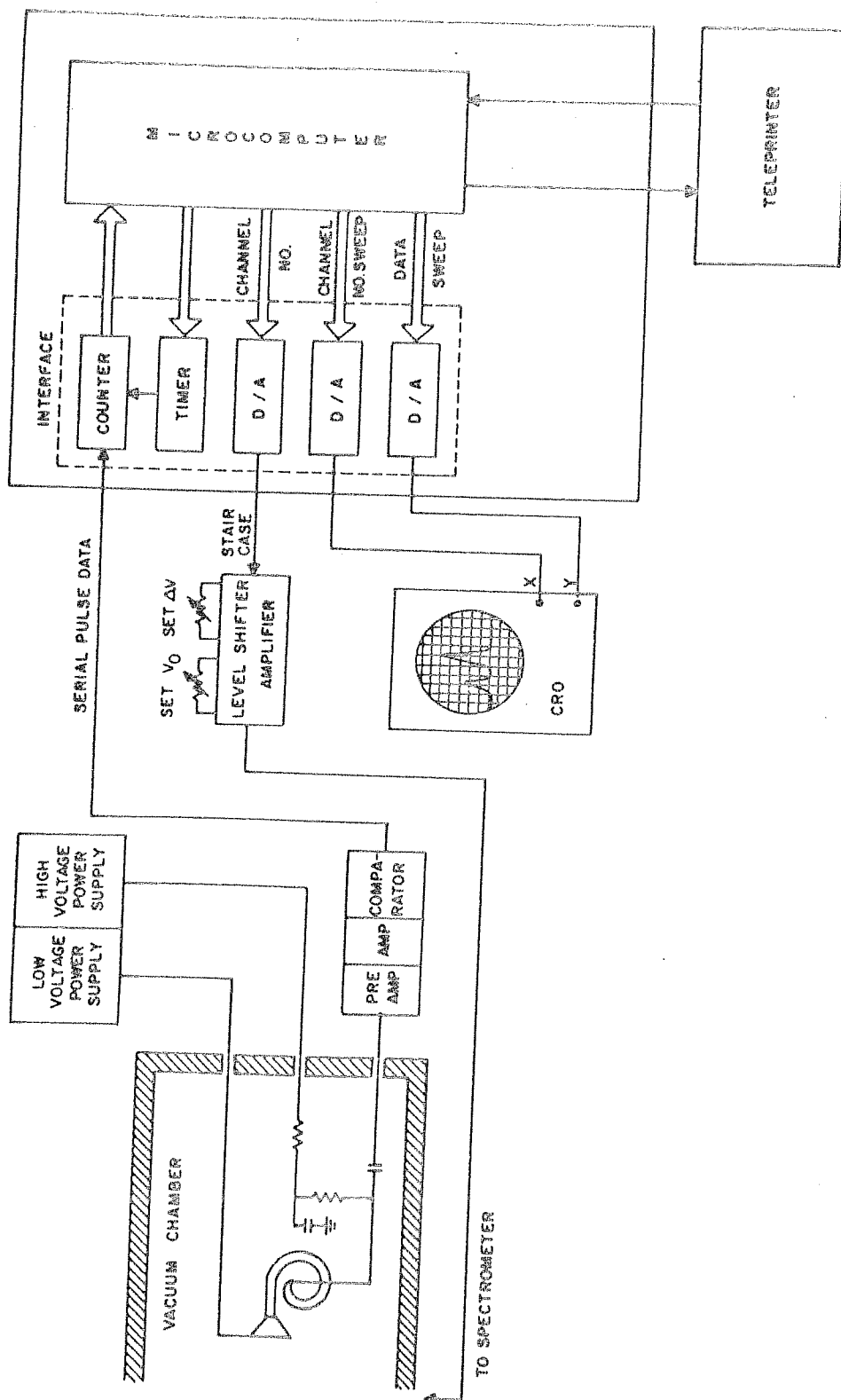
For better performance and stability of the sensor, the head was maintained at an elevated temperature of 318 K. This facility was provided in the unit by the manufacturers.

2.8 Data acquisition system

The data collection was automated by using a microcomputer controlled multichannel analyser (256 channels) which was made in our laboratory. Functions of this MCA were to select data collection mode through external commands, acquire data, display data on a CRO, generate a stair-case voltage and print out the data on a teleprinter. The block diagram of the data acquisition system is shown in figure 2.9.

The MCA consisted mainly of two units: i) a microcomputer and ii) an interface unit. The microcomputer was programmed to function as an MCA, with 256 channels for data storage and 2^{16} counts storage capacity per channel. It used a teleprinter to read in commands and print out data.

FIG.2.9 BLOCK DIAGRAM OF DATA ACQUISITION SYSTEM



The interface consisted of a pulse counter, a timer and three digital to analog converters (D/A). The computer controls the timer to generate a pulse of predetermined width. This gate pulse enables the counter to count the incoming serial pulse data from the experiment. At the end of this gate pulse, the number of counts were stored in respective channel memory of the microcomputer. The channel number was advanced and a fresh trigger pulse was sent to the timer. The channel number was fed to a precision D/A converter which produced a d.c. voltage proportional to the channel number fed in and this output served as the staircase voltage for the experiment. A fast scan of each channel data along with its corresponding channel number was continuously fed to two other D/A converters which produced x and y sweep voltages for an external CRO, thus producing a steady display of spectrum.

A level-shifter amplifier was used to shift the level, V_0 , of the staircase and to amplify/attenuate the voltage stepsize ΔV . V_0 could be set anywhere between +30 and -30 V and ΔV could be chosen in any stepsize ranging from 2 to 200 mV. Apart from these two functions, the level shifter amplifier inverted the staircase, thus producing a negative staircase, which generates the photoelectron spectrum in the increasing order of energy along the x-axis.

To start the data collection, initial voltage V_0 and voltage stepsize, V were fixed manually through the level shifter amplifier. The teleprinter commands were given to the microcomputer to select the data collection time per channel (gate), number of scans required and mode of collection of data. Gate could be set from any of 0.1, 1, 10, 20, 100, 200 and 300 seconds. Number of scans could be chosen from any number greater than 0 and less than 100, and in mode of operation, channelwise addition or subtraction of data was possible in successive scans. Once data collection started, the status of spectrum was displayed simultaneously on the CRO. Acquisition stops as soon as all the commands were fulfilled. It was possible to abort or suspend data collection during acquisition, preserving the current contents of the memory. Some of the other commands to the microcomputer were to erase the memory (refresh), enhance or truncate the display, print or punch out the data etc.

At the end of each run, the data was either printed out or punched on a paper tape.

2.9 Operation of the photoelectron spectrometer

The photoelectron spectrometer was operated in two different modes. These two different modes were achieved by applying the staircase voltage on different parts of the electron spectrometer. These modes were called 'grounded mode' and 'accelerated mode'.

As the name suggests, in the grounded mode, the inner electrode was grounded and the scanning voltage was applied on the outer cylinder of the CMA. The initial value of the negative staircase, V_0 , was chosen in such a way that, even the electrons with least energy in the spectrum were focussed away from the exit slit of the inner cylinder. Voltage stepsize ΔV was appropriately chosen. With the increase in scanning voltage (in negative direction), the photoelectron spectrum built up in increasing order of electron energy. The collection efficiency of the spectrometer operated in grounded mode was found to be low for electron energies less than 2 eV, but above 2 eV, it remained almost constant.

In accelerated mode, the staircase voltage was applied on the inner electrode and a constant negative bias voltage, V' , was applied on the outer cylinder of the CMA. This voltage, V' , was so chosen that even the electrons with maximum energy in the spectrum were focussed before the exit slit on the inner cylinder of the CMA. This bias voltage was derived from a nickel-cadmium battery along with multiturn, precision potentiometer. If the staircase voltage is positive, then it will retard, and if it is negative, it will accelerate the electrons in the accelerating region. Thus in this mode of operation of the spectrometer, the spectrum built up in the decreasing order of electron

energy, i. e. higher energy component of spectrum appeared first followed by the lower energy component. The collection efficiency of the spectrometer, operated in this mode, increases phenomenally below 1.5 eV and above 1.5 eV, it assumes almost a constant value. Advantages of accelerated mode over grounded mode were large collection efficiency at low electron energies and maintaining the same energy resolution throughout the photoelectron spectrum.

A third method tried out was a combination of the two methods discussed above. In this method, the scanning voltage was applied on the outer cylinder and a constant boost voltage, derived from nickel-cadmium battery, was applied on the inner electrode. This shifted the whole spectrum through a definite energy value. This method was used especially in the region of 1 to 2 eV. This was the region, where it became difficult to choose the grounded mode or accelerated mode because of collection efficiency considerations.

However, it must be pointed out here that, the results of the present experiment did not depend on either the mode of operation or the collection efficiency of the spectrometer. The spectrometer was used in any of these three modes frequently, so as to get large photoelectron signal in respective electron energy regions.

2.9.1 Performance of the spectrometer

Figure 2.10 shows the photoelectron spectrum of argon and nitrogen using 58.4 mm HeI radiation for photoionisation. In the photoelectron spectrum of N_2 , vibrational levels corresponding to $A^2\Pi_u$ state of the molecular ion have only been shown. The spectrometer was operated in grounded mode for both these spectra. The resolving power achieved, on average, was better than 100.

2.10 Scattering by target atoms

Before the photoelectrons produced in the ionising region by the interaction of VUV photons with source gas emerged out into the accelerating and analysing regions, they were allowed to travel in the target gas medium. The target gas for scattering studies could be the same as the source gas used for the production of photoelectrons itself, or any different gas. In both these cases, scattering takes place, resulting in change of the amplitudes of the peaks in the photoelectron spectra at different gas pressures. But, since the production rate of electrons is also involved when source and target gas are the same, the pressure versus intensity curve of the photoelectron peak differs drastically from that when source gas is different from target gas.

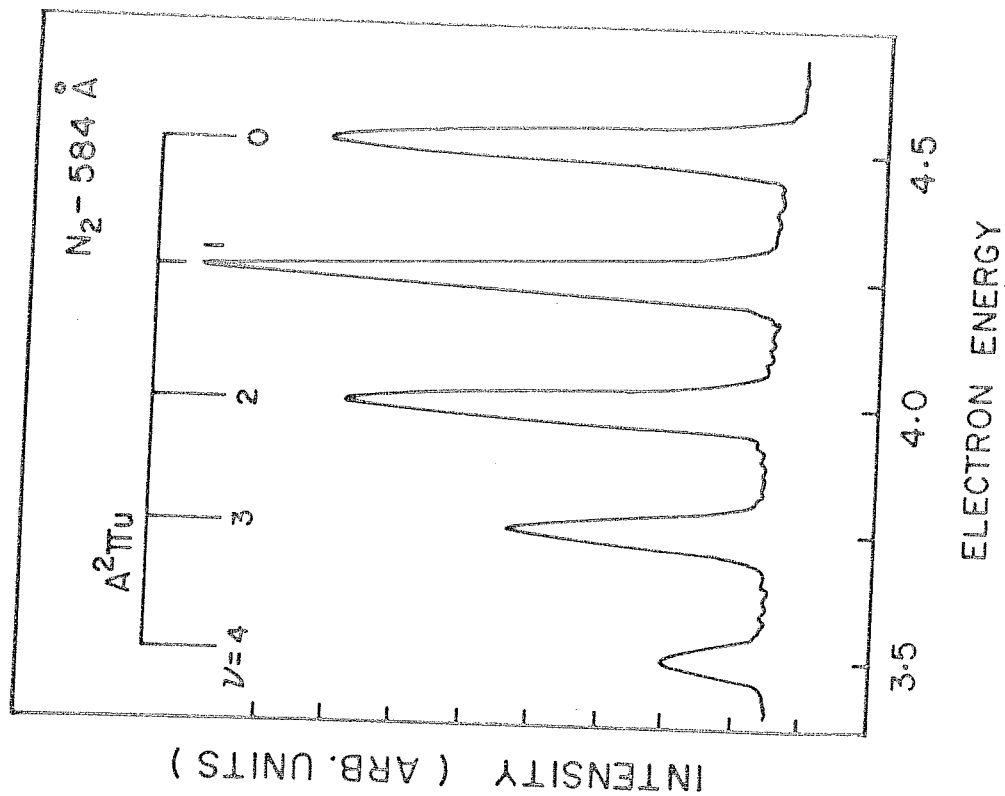
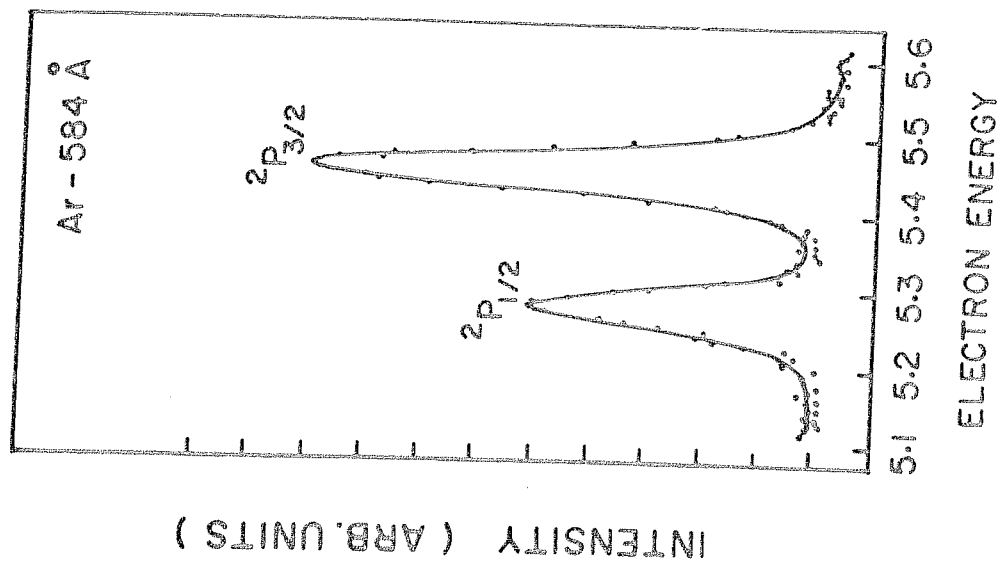


FIG. 2.10 PHOTOELECTRON SPECTRA OF ARGON AND NITROGEN USING 584 Å RADIATION

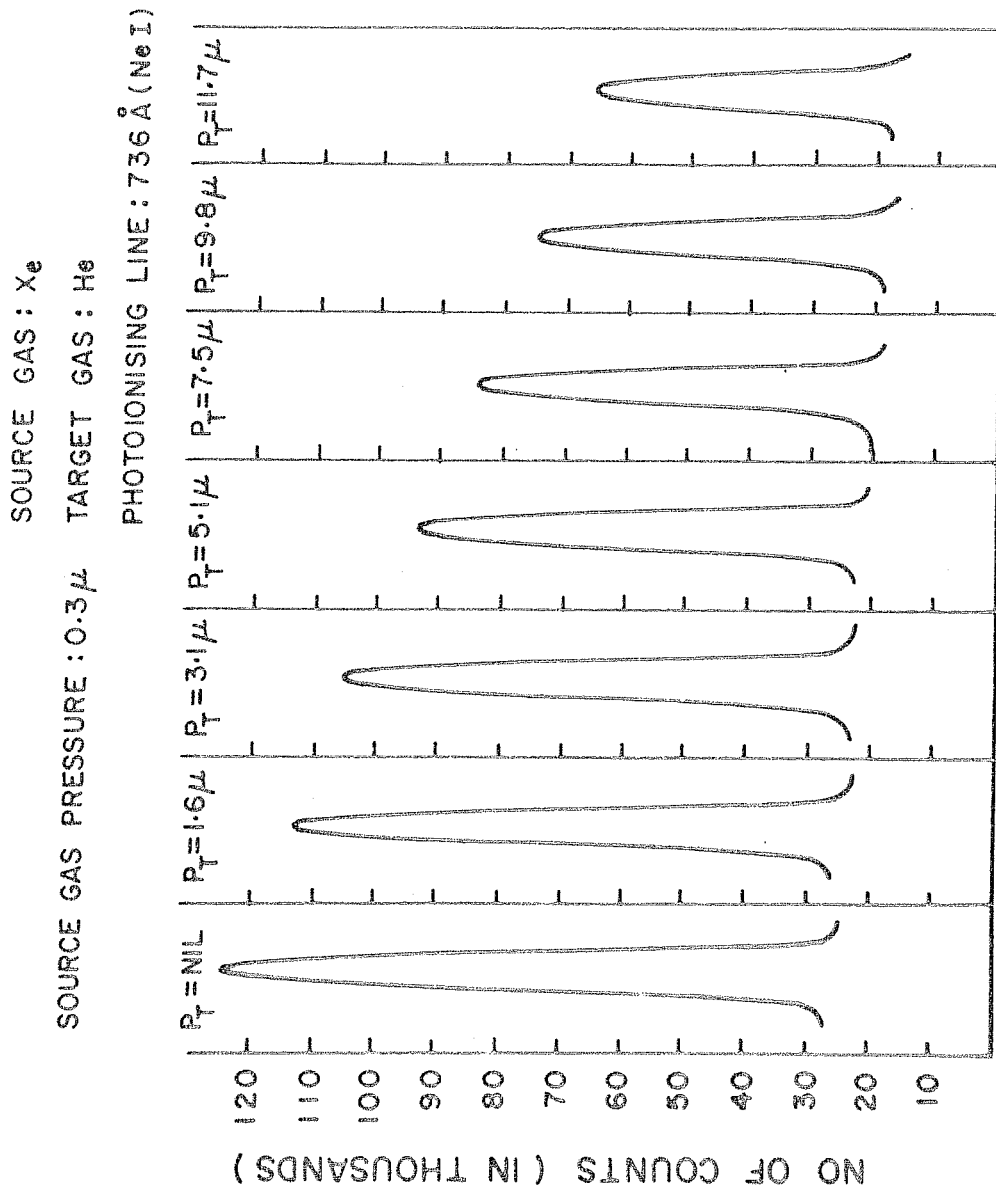
2.10.1 When source and target gases are different

In this case, the partial pressure of the source gas was kept constant throughout the experiment. When target gas was introduced into the ionising region itself, it did not vary the electron production rate. Any decrease in amplitude of the photoelectron peak was due to the scattering of electrons by the target gas present in the scattering region. Scattering due to source gas itself was small, and moreover, it did not propagate into the derivation of scattering cross-section for the target gas. The curve for intensity of a particular photoelectron peak versus target gas pressure will be an exponential curve, and the characteristic slope of such a curve would depend on the scattering cross-section of target gas species at that particular electron energy. The variation of amplitudes of photoelectron peak of argon ($^2P_{3/2}$ state of ion and 736 Å Ne I radiation) with increase of helium gas pressure in the scattering region is shown in figure 2.11

2.10.2 When source and target gas are same

In this case, the pressure of the source gas itself was varied to study the scattering cross-section in the source gas. Photoelectron production is related to the pressure of source gas present in the ionising region. Therefore, at low gas pressures, amplitude of the photoelectron peak increases

FIG.2.11 VARIATION OF $X_e^2 P_{1/2}$ PEAK WITH
HELIUM GAS PRESSURE IN THE
SCATTERING REGION



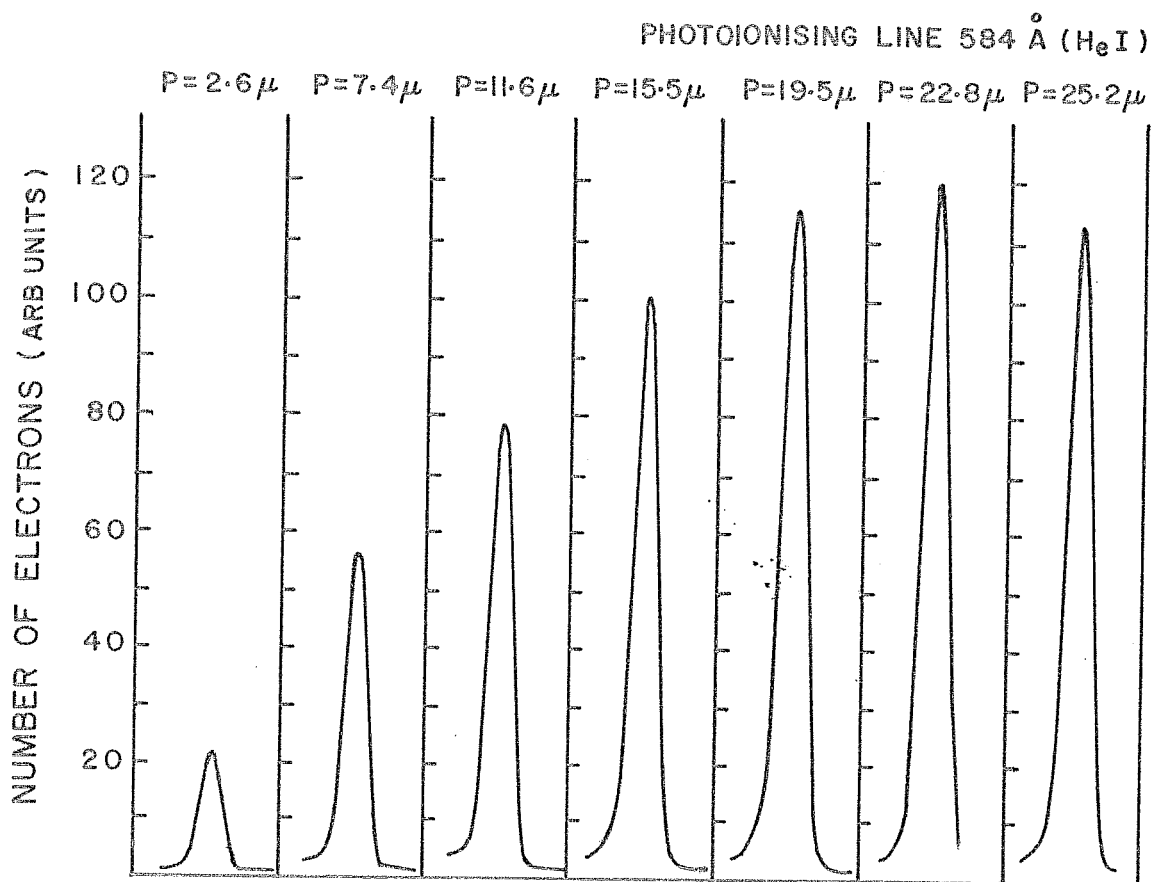


Fig. 2.12 VARIATION OF $\text{Ar } ^2\text{P}_{3/2}$ PEAK WITH ARGON GAS PRESSURE IN THE SCATTERING REGION

linearly with source gas pressure. At higher pressures, because of scattering of electrons by source gas itself, there was a departure from linearity in the intensity versus pressure curve. At very high pressures, the curve even dropped down. It is possible to calculate scattering cross-sections from such departure from linearity of the curve. Figure 2.12 shows the variation of $^2P_{3/2}$ peak of argon due to 584 \AA He I, with the increase of argon gas pressure in the scattering region.

CHAPTER THREE

METHOD FOR CALCULATION OF SCATTERING CROSS-SECTIONS

As described in the previous chapter, the electron scattering cross-sections for noble gases measured using a photoelectron source have been calculated from the observed attenuation of peaks in the photoelectron spectra, occurring due to the introduction of target gas in the ionising region. Two different analysis procedures have been used depending upon the nature of the source and target atoms.

The present method is very much different from the method adopted by Kumar and Krishnakumar [1981b] for the measurement of electron scattering cross-section of

molecular hydrogen. This method would be described here briefly to bring out the basic differences in the procedures adopted in the two cases.

In their experiment, seven discrete electron energies from 0.02 to 1.14 eV were available at which electron-hydrogen cross-section were measured. The electrons were produced by the photoionisation of hydrogen molecule by NeI (736 Å) photons and the electron energies corresponded to the difference of photon energy and the ionisation potentials of vibrational levels of $V' = 0$ to $V' = 6$ of the ground state of the hydrogen ion. In this case the source and target gas were the same. Photoelectron spectra were recorded at various pressures of hydrogen, but, unfortunately, the pressures were not measured absolutely in the ionising region. The pressure versus intensity curve for the photoelectron peak corresponding to $V' = 3$ level of ground state of the hydrogen molecular ion is reproduced here in figure 3.1. It can be seen that on the low pressure side, the photoelectron intensity bears almost a linear relationship with the pressure of the target gas in the ionising region. However, at higher pressures, because of scattering in the same region, there is departure from the linearity, and at still higher pressures, the amplitude of photoelectron peak gets reduced. This is represented by curve III in figure 3.1. Curve I is extrapolation of the linear part at low pressures and it represents the number of electrons available for scattering, I_{e0} . However, curve I

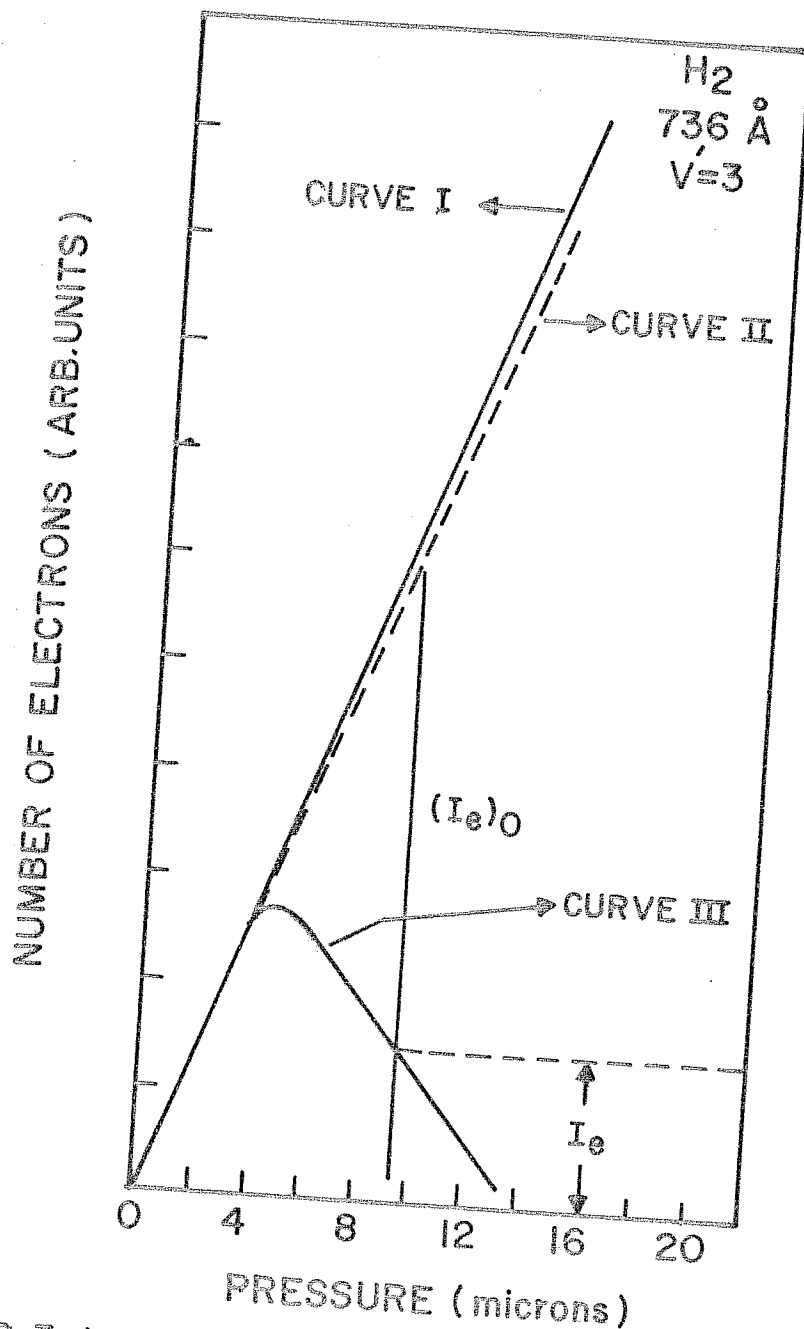


FIG.3.1 e-H₂ SCATTERING PRESSURE VERSUS
 INTENSITY OF PHOTOELECTRON PEAK
 [KUMAR AND KRISHNAKUMAR 1981 b]

has to be modified by a small amount, taking into account the variation of photon intensity due to its absorption by target gas. Curve II in figure 3.1 is obtained by applying the said correction on curve I. I_{eo} and I_e which are the initial and final intensities of the photoelectron peak are extracted from curve II and curve III respectively as shown in the figure. These values of I_{eo} and I_e were used in the Beer-Lambert law and relative cross-sections were computed. The cross-sections were then made absolute by normalizing at a single electron energy, where absolute cross-sections were available from other experiments.

This method had a few limitations. Firstly, the electron scattering cross-sections for only a few gases could be measured, whose cross-sections are sufficiently large so as to show appreciable departure from linearity in the curve III, mentioned earlier. Secondly, any change in light intensity during the experiment directly reflected in the measured values of cross-section. In view of this, an analytical method was developed to calculate the scattering cross-sections in the present experiment. This method incorporates correction for the peak amplitude due to the possible variation in light intensity during the experiment. Two different methods have been adopted; one when the source and target gases are different and the other when they are the same. Both of these methods are described in the following sections.

3.1 When source and target are different

In this method the gas used to produce photoelectrons for scattering studies was different from the target gas under investigation. The partial pressure of the source gas, P' was maintained at a low and constant value throughout one set of data collection. Thus the number of electrons available for scattering was maintained constant throughout one set of observation. Target gas was introduced into the ionising region and the partial pressures of the target gas were measured absolutely as P_1, P_2, \dots by measuring the total pressure. Reduction in intensity of the photoelectron peak were also subsequently measured.

The reduction in the amplitude of the photoelectron spectra due to the presence of target gas species in the ionising region is related to the initial intensity, I_{e0} , by Beer-Lambert law. The decrease in intensity of the electron beam, dI_{e0} , due to its passage through an infinitesimal distance, dx , is proportional to the intensity of the beam at the position x , $I(x)$, number density of scattering medium, n , and the total scattering cross-section of the scattering medium, Q .

$$-dI = I(x)nQdx$$

$$\text{or } \text{Log}(I) = -nQx + C$$

Applying boundary conditions $I|_{x=0} = I_{e0}$ and $I|_{x=x} = I_e$, the above equation can be written as

$$I_e = I_{e0} \exp(-nQx) \quad \text{-----} \quad (3.1)$$

This law is valid only for isotropic and homogenous scattering medium. Another condition to be satisfied for the validity of this law is that, electrons in the beam are scattered only once during their passage through the scattering medium.

The following set of parameters are used in the course of derivation for scattering cross-section:

- P_1 - Partial pressure of source gas inside the ionising region.
- $P_1, P_2 \dots$ - Partial pressures of target gas inside the ionising region.
- P_1 - Partial pressure of source gas outside the ionising region.
- $P_1, P_2 \dots$ - Partial pressures of target gas outside the ionising region.
- Q_s - Total scattering cross-section for the source gas.
- Q_t - Total scattering cross-section for the target gas.
- σ_s - Ionisation cross-section for source gas.
- σ_t - Ionisation cross-section for target gas.
- k_s - Photoabsorption coefficient of source gas.
- k_t - Photoabsorption coefficient of target gas.

The number density of gas inside the ionising region is expressed in terms of Loschmidt's number n_0 and measured pressure expressed in Torr,

$$n = \frac{n_0 P}{760}$$

where $n_0 = 2.688 \times 10^{19} \text{ cm}^{-3}$.

For two pressures of the target gas P_1 and P_2 , the observed intensities I_{e1} and I_{e2} are given by

$$I_{e1} = I_{e01} \exp \left[-\frac{n_0}{760} (P_1 Q_s + P_1 Q_t) \right]$$

$$I_{e2} = I_{e02} \exp \left[-\frac{n_0}{760} (P_2 Q_s + P_2 Q_t) \right]$$

where $x = 2.37 \text{ cm}$, the physical path length (see figure 3.2).

Or

$$\frac{I_{e1}}{I_{e2}} = \frac{I_{e01}}{I_{e02}} \exp \left[-\frac{(P_1 - P_2)}{760} n_0 Q_t x \right] \quad \text{--- (3.2)}$$

The variation in I_{e0} could be due to variation of light intensity (or source gas pressure) or due to the absorption of VUV photon in other parts of the system.

In figure 3.2, photoelectrons produced in the shaded area along the photon path (extended length = Δl) are only admitted to analysing region, and finally registered as signals. Number of electrons produced in this region is related to number density of source gas, n , average photon intensity of VUV photon in this region, $\langle I_\lambda \rangle$, ionisation cross-section of source gas, σ_s and the extent of length, l . It is assumed that the photon intensity does not vary over the distance Δl , which is essential for writing down the expression

$$I_{e0} = n \langle I_\lambda \rangle \sigma_s \Delta l$$

which gives

$$\frac{I_{e01}}{I_{e02}} = \frac{\langle I_\lambda \rangle_1}{\langle I_\lambda \rangle_2} \quad \text{--- (3.3)}$$

The photon absorption is also governed by Beer-Lambert law

$$I_\lambda = I_{\lambda 0} \exp [-n \sigma_a l]$$

where σ_a is the photo absorption cross-section, $I_{\lambda 0}$ is the

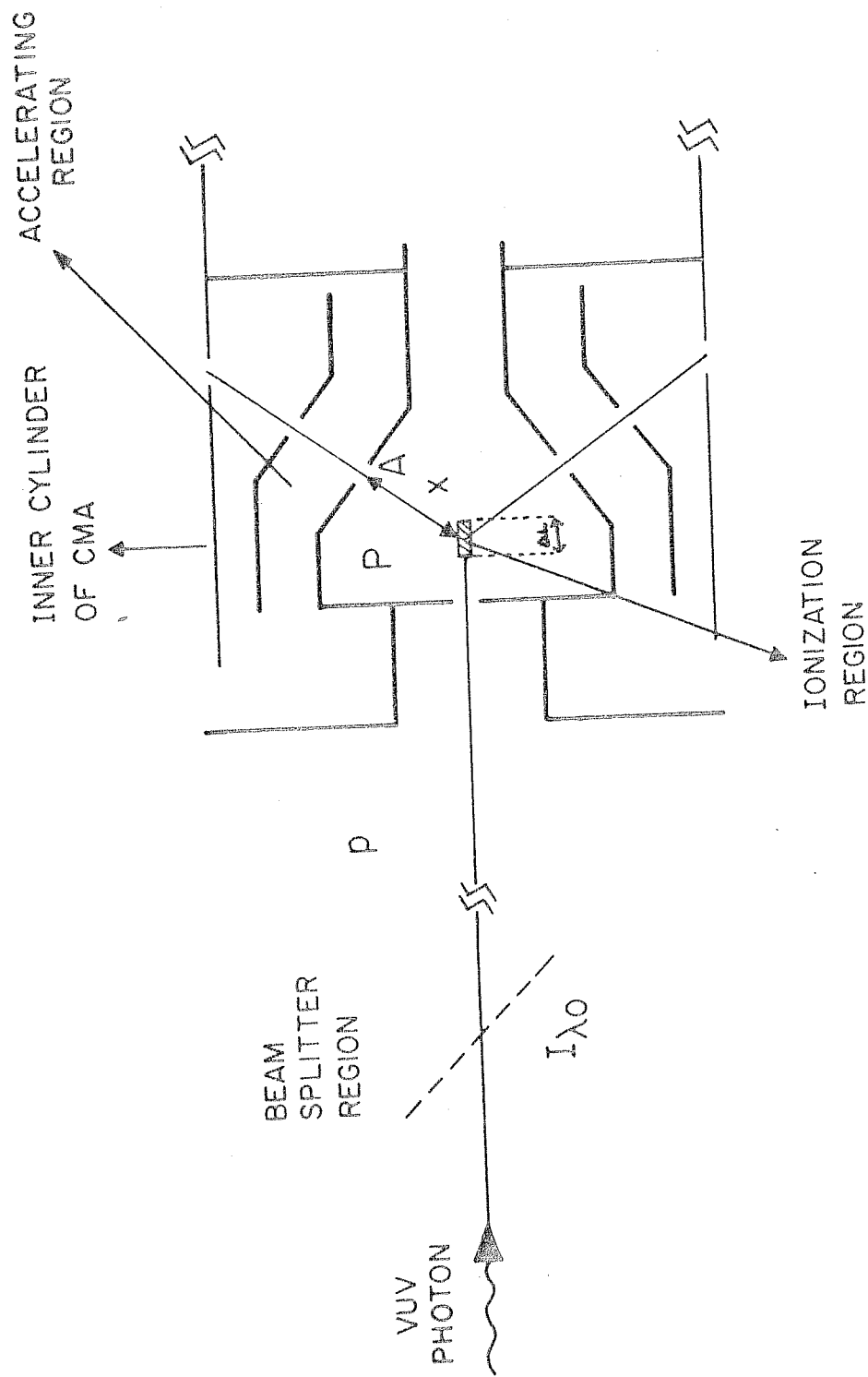


FIG.3.2 SCHEMATIC DIAGRAM OF IONISING AND SCATTERING REGIONS

incident intensity of the photon beam measured at the beam-splitter and l is the "effective pathlength" from this point to the ionising region represented by shaded area in the figure.

Since $k_a = n_0 \times \sigma_a$, we can write

$$\langle I_\lambda \rangle_1 = I_{\lambda 01} \exp \left[-\frac{K_s}{760} (P'l_2 + P'l_1) - \frac{K_t}{760} (P_1 l_2 + P_2 l_1) \right]$$

$$\langle I_\lambda \rangle_2 = I_{\lambda 02} \exp \left[-\frac{K_s}{760} (P'l_2 + P'l_1) - \frac{K_t}{760} (P_2 l_2 + P_1 l_1) \right]$$

$$\text{or } \frac{\langle I_\lambda \rangle_1}{\langle I_\lambda \rangle_2} = \frac{I_{\lambda 01}}{I_{\lambda 02}} \exp \left[-\frac{K_t}{760} \{ l_2 (P_1 - P_2) + l_1 (P_1 - P_2) \} \right] \quad (3.4)$$

where l_1 and l_2 are lengths shown in fig.3.2.

In section 2.6.1, the variation of pressure outside the ionising region with respect to variation of pressure inside has been investigated, and it has been established that the relation is linear in a wide range of pressures. It has also been established that $p = aP$, value of 'a' being 0.124 in the pressure region from 10^{-3} to 5×10^{-2} Torr.

Using this in the equation (3.4),

$$\frac{\langle I_\lambda \rangle_1}{\langle I_\lambda \rangle_2} = \frac{I_{\lambda 01}}{I_{\lambda 02}} \exp \left[-\frac{K_t}{760} (P_1 - P_2) (al_1 + l_2) \right] \quad (3.5)$$

Using equation (3.5) in (3.3) we get

$$\frac{I_{e01}}{I_{e02}} = \frac{I_{\lambda 01}}{I_{\lambda 02}} \exp \left[-\frac{K_t}{760} (P_1 - P_2) (al_1 + l_2) \right] \quad (3.6)$$

Substituting (3.6) in (3.2) we get

$$\frac{I_{e1}}{I_{e2}} = \frac{I_{\lambda 01}}{I_{\lambda 02}} \exp \left[-\frac{(P_1 - P_2)}{760} \{ n_0 Q_t x + K_t (al_1 + l_2) \} \right] \quad (3.7)$$

or

$$\ln \left[\frac{I_{e2}}{I_{e1}} \frac{I_{\lambda 01}}{I_{\lambda 02}} \right] = \frac{P_1 - P_2}{760} [n_0 Q_t x + K_t (al_1 + l_2)] \quad (3.8)$$

It must be pointed out here that, though absolute values of $I_{\lambda 0}$ cannot be determined by the beam-splitter, the ratio $I_{\lambda 01}/I_{\lambda 02}$ could be determined from the beam-splitter

readings.

The correction term $k_t (a l_1 + l_2)$ could be neglected in cases where the energy of the photon beam is such that it cannot ionise the target gas (for example, NeI 736 Å line in helium). In other cases the absorption coefficients are taken from literature and necessary corrections were applied. The values used for absorption coefficients in various cases are presented in table 3.1. References are also given there.

The logarithms on L.H.S of equation (3.8) plotted against $(P_1 - P_2)$ are straight lines as suggested by equation (3.8). The slopes of these lines represent the scattering cross-sections at different energies.

3.2 When the source and target gas are same

In this method, source and target gas are the same as in the case of measurement of electron cross-sections for argon when source gas for producing photoelectrons is argon itself. The set of parameters used in the course of derivation for scattering cross-section is same as used in section 3.1, except that no primes (') and sub/superscripts are used to differentiate target from source.

In this method the observed intensity of the peak in photoelectron spectrum is decided by two competing

Table 3.1 Values of absorption coefficients for noble gases in VUV region

<u>Target gas</u>	<u>VUV photon</u> (Å)	<u>Absorption coefficient</u> (cm ⁻¹)	<u>Reference</u>
Helium	584	--	
	736	---	
	744	--	
Neon	584	141.2	Ditchburn [1960]
	736	--	
	744	--	
Argon	584	983.0	Cairns and Samson [1965] Rustgi [1964] " " "
	736	940.0	
	744	940.0	
Krypton	584	900.0	Metzger and Cook [1965] " " " " " " " "
	736	1050.0	
	744	1050.0	
Xenon	584	650.0	" " " " " " " " " " " "
	736	1175.0	
	744	1175.0	

processes, viz. electron production rate and electron scattering. Production rate is linearly proportional to number density of gas atoms (or pressure), where as scattering is related to inverse of exponential of pressure. Actual detected intensity is product of these two.

$$I_e \propto P e^{-\lambda P}$$

where λ is a parameter involving the scattering cross-section.

For such a function, there exists a critical pressure, P_c where $\left. \frac{dI_e}{dP} \right|_{P=P_c} = 0$, and this corresponds to the turning point of I_e versus P curve. One of such curve (He I 584 Å in argon) is shown in figure 3.3. It could be noted that, P_c is depending upon the scattering cross-section.

To get an analytic expression for scattering cross-section, we exactly follow the analysis on the same lines as given in the previous section. For two pressures P_1 and P_2 in the ionising region

$$\frac{I_{e1}}{I_{e2}} = \frac{I_{e01}}{I_{e02}} \exp \left[- \frac{(P_1 - P_2)}{760} n_0 Q x \right]$$

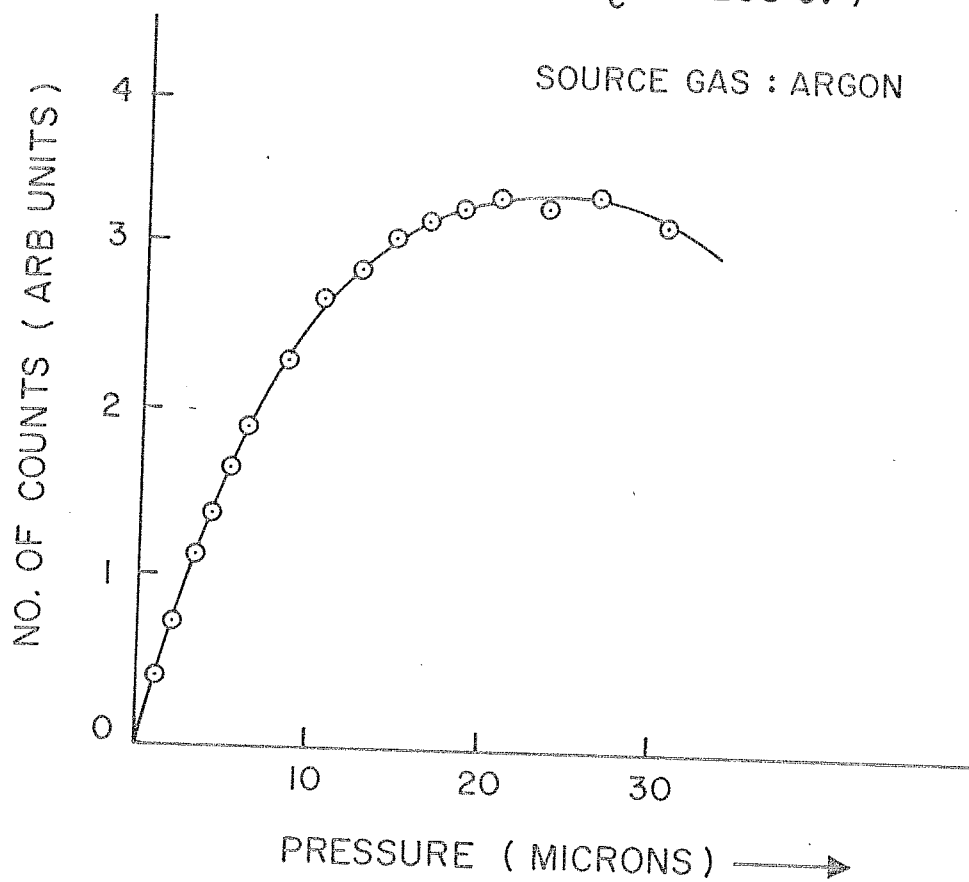
which is same as equation (3.2) in previous section. In this case, I_{e01} and I_{e02} are very much different in values, because electron production rates are altered because of variation of source gas pressure in the ionising region. The terms I_{e01} and I_{e02} become pressure dependent such that

$$\frac{I_{e01}}{I_{e02}} = \frac{P_1 \langle I \rangle_1}{P_2 \langle I \rangle_2}$$

To get the ratio $\langle I \rangle_1 / \langle I \rangle_2$, we proceed on the same lines as done earlier.

$$\frac{I_{e01}}{I_{e02}} = \frac{P_1}{P_2} \frac{I_{\lambda 01}}{I_{\lambda 02}} \exp \left[- \frac{K}{760} (P_1 - P_2) (\alpha l_1 + l_2) \right] \quad \dots (3.10)$$

Fig. 3.3 SCATTERING OF PHOTOELECTRONS
IN ARGON ($E_e = 5.283 \text{ eV}$)



Substituting this in equation (3.9) and finally in (3.2) we get

$$\frac{I_{e1}}{I_{e2}} = \frac{P_1}{P_2} \frac{I_{\lambda e1}}{I_{\lambda e2}} \exp \left[\frac{-(P_1 - P_2)}{760} \{ n_c Q x + k(a l_1 + l_2) \} \right]$$

or

$$\ln \left[\frac{I_{e2}}{I_{e1}} \frac{P_1}{P_2} \frac{I_{\lambda e1}}{I_{\lambda e2}} \right] = \frac{P_1 - P_2}{760} [n_c Q x + k(a l_1 + l_2)] \quad \text{--- (3.11)}$$

Here also graphs between the logarithms on L.H.S of equation (3.11) versus $(P_1 - P_2)$ are straight lines, the slope of the curve being related to the scattering cross-section. But, it must be noted here that the arguments of the logarithm contain pressure of the source/target gas as a variable.

All parameters I_{e1} , I_{e2}, P_1 , P_2 the ratios $I_{\lambda o1}/I_{\lambda o2}$ and 'a' were accurately measured in the experiment. Various lengths x , l_1 and l_2 are known from the geometry of the system. Relevant photoabsorption coefficients are taken from literature. The formulae (3.8) or (3.11) were used to find out the cross-sections depending on the two cases.

CHAPTER FOUR

ERROR ANALYSIS

The errors in the present experiment for the measurement of electron scattering cross-section can be conveniently classified as multiplicative, additive and shape errors. A close inspection of Beer-Lambert law

$$I_e = I_{e0} \exp [-nQx]$$

which is the law governing the total scattering, reveals that errors arising from uncertainty in pressure, temperature or scattering path length fall under multiplicative errors, whereas errors because of counting statistics, drift in source gas pressure and variation in light intensity during the experiment come under additive

errors. The shape errors are mainly caused by forward scattering and multiple scattering of electrons in the scattering cell. Other sources of errors like gas impurities, scattering of electrons by ionic species and uncertainty of electron energy also contribute to shape errors, though in a small way. Coherent sum of all these errors would act as the upper limit for all errors in the experiment. The incoherent sum is obtained by adding squares of all errors and taking square root of the sum. This would represent the most probable error in the experiment. In the following sections, a complete description of all these errors would be given, so as to find out the upper limit estimate to the actual error and the most probable error in the present experiment.

4.1 Pressure measurement

The total error in the pressure measurement could be attributed to errors due to instrumental calibration, reference pressure and drift in null reading of the pressure meter.

4.1.1 Instrument calibration

The gas pressure was measured absolutely by means of an MKS Baratron capacitance manometer (310 BH-1). This had a sensor head capable of measuring to a maximum of 1 Torr absolutely, provided the reference side of the head was evacuated to a high degree of vacuum. In the experiment, the

usual range of pressures to be measured absolutely was from 10^{-3} to 2.5×10^{-2} Torr. The system error given by the manufacturer was $\pm 0.15\%$ and 0.09% at these two extreme ends. As an upper limit to the actual error, $\pm 0.15\%$ was chosen as the error due to the instrument calibration in all pressure ranges (i.e. about 10^{-3} Torr) and this value was used to calculate the most probable error.

As it was not possible to measure gradients along the scattering path due to other considerations (like problems of contact potentials inside the scattering region), it was minimised in the following way. The conductance of the gas feeding line to the ionising region was chosen to have a larger value than that of the slit around the ionising region. This apparently helped to reduce the pressure gradients from the gas inlet port to the exit slit. This particular consideration along with vigorous differential pumping above the slits of the ionising region, brought the pressure inside to an equilibrium value with negligible gradients. It may be pointed out here that the source and target gases were pre-mixed (immediately after the fine control valves) to avoid any anisotropic composition of gas mixture inside the ionising region, when source gas used was different from target gas.

By virtue of balancing valve (see figure 2.8), it was possible to obtain null reading in the MKS Baratron capacitance manometer before starting the experiment. After

the experiment also, the sensor head was balanced to make sure that null reading did not drift much. Therefore, error due to the drift in null reading of the Baratron capacitance manometer could be ignored.

4.1.2 Reference pressure

The reference side of the MKS Baratron was continuously evacuated using an oil diffusion pump (pumping speed 170 lit.Sec⁻¹) with a liquid nitrogen trap. The vacuum obtained in the reference side was always better than 10^{-5} Torr (usually ranging from 5 to 7×10^{-6} Torr). Since the pressure measured using this gauge was always greater than 10^{-3} Torr, which was at least two orders of magnitude larger, the errors introduced because of reference side pressure were negligible.

4.2 Thermal transpiration

The temperature of the capacitance manometer sensor head was maintained at 318 K, while the temperature of the scattering cell was usually room temperature (300 K). Thus we might expect the pressure in the scattering chamber to be slightly less than the pressure indicated by the MKS unit head due to thermal transpiration effects. The effects of thermal transpiration in the present work have been

calculated on the lines suggested by Edmonds and Hobson [1965]:

$$P_s = a (T_s/T_m)^{1/2} P_m \dots\dots\dots (4.1)$$

where P_s and T_s were the pressure and temperature in the scattering region, P_m , pressure indicated by the MKS sensor head, and 'a' is a constant which depends on the geometry over which the temperature gradients occur. For an ideal aperture, $a \approx 1$, but in practice, it may have a value slightly greater than unity. From equation (4.1), we find that the pressure in the scattering chamber has to be revised upwards by 2.9%. This pressure correction has been made in all our measurements and scattering cross-sections have been calculated accordingly. The only other error which occurred was due to the uncertainty in temperature in the scattering region. This could be as high as $\pm 1^\circ\text{C}$ and the corresponding error in determining the pressure is estimated to a maximum of $\pm 0.4\%$.

4.3 Uncertainty in scattering path length

The scattering path length in the experiment was the distance between the centre of photoionising region (shaded region in figure 3.2) to the exit slit. This distance was exactly measured from the geometry of the scattering cell. Even though the angles involved in its structure were accurate upto fraction of a degree, allowing $\pm 1^\circ$ variation in the angles, it was found that the calculation of

scattering path length would vary only by $\pm 0.7\%$. Further uncertainties are due to extension of the photon beam along the gas column (represented by 1 in figure 3.2) and finite width of the photon beam in the ionising region. Geometrical calculations showed that, the error introduced due to the extension of photon beam in the gas column was $\pm 0.26\%$ and due to the finite dimension of photon beam, the introduced error was $\pm 1.1\%$. Thus, total uncertainty in determining scattering path length was chosen as $\pm 2.1\%$.

4.4 Counting statistics

Since electron counting is basically a statistical process, it will have a Poissonian distribution. This introduces an uncertainty of $\pm \sqrt{N}$ to the actual number of counts N . To reduce this uncertainty, it is advisable to have large number of counts. Usual number of counts per channel at the electron peaks were of the order of 10^4 . The limiting factor for this was the storage capacity per channel in the MCA, which was $(2^{16}-1)$. (In some cases overflow spectrum at the peaks also were recorded, thus allowing maximum number of counts upto $(2^{17}-1)$). When the signals were weak, collection time/channel was chosen to be high enough to give number of counts of this order.

The spectrum recorded with no gas present in the ionising region was taken as the background level. Usually these were metal electrons, and were subtracted from the

photoelectron spectra. Strictly speaking, area under the peak (between rising and falling edges of the peak above the background) represent the intensity of electron at that particular energy. But assuming that the peaks were triangular in shape, and maintaining constant energy resolution of the energy analyser during one complete set of data collection (to maintain the base of the triangle constant), the height of the peak would exactly represent the intensity. Both these methods were tried out and no appreciable difference was observed in the results. In each case, the resolution of the spectrometer was so chosen, as to have at least a few distinct points around the peak, to decide the position and intensity of the peak without ambiguity.

Drift in source gas pressure also changes the initial intensity of the electrons. To overcome this problem, source gas was introduced into the system at least one or two hours before introducing the target gas. This helped the source gas pressure to get stabilized.

The third problem was the variation of VUV photon intensity during the experiment. Though, the variation could be monitored by means of beam-splitter, it was necessary to have further check on the data. At each pressure point of the target gas, minimum three readings of the same electron peak were taken. If the level of disagreement of this data was greater than 1%, then the data was rejected.

The total uncertainty due to counting statistics was estimated as +1.5%.

4.5 Forward scattering

An error, inherent to all transmission experiments, results from the failure to sufficiently discriminate against electrons scattered by the sample gas in the forward direction. Forward scattering can lead to a significant reduction in the measured cross-section. This error is maximum, at higher energies, where inelastic and elastic scattering are dominated by small angle scattering. Usual procedures accepted to quantify the forward scattering experimentally are by varying the acceptance angle of the detector [Jones and Bonham, 1982; Jones, 1985] or by changing the electron beam direction through small angles [Blaauw et al, 1977]. Alternately, forward scattering could be estimated by modelling. Blaauw et al [1977] derived the cross-sections from the equation.

$$\frac{I_2}{I_1} = \exp \left[-nQL + n(L d\Omega)_{\text{eff}} \frac{d\sigma(\theta=0)}{d\Omega} \right] \quad (4.2)$$

where $\frac{I_2}{I_1}$ is the ratio of electron intensities with and without gas in the scattering cell, L is the scattering path length and other parameters have usual meaning.

In the present experiment, it was difficult to vary the acceptance angle of the detector or to change the direction

of the electron beam. Since the electron energy domain is low (elastic limit) for all target atoms under investigation, the error arising from forward scattering also would be low. An error of $\pm 0.5\%$ was attributed because of forward scattering which is much higher than the attributed error in this energy range by other investigators.

4.6 Multiple scattering

It has been discussed earlier, that for the validity of Beer-Lambert law, the pressure of the target gas must be sufficiently low as to avoid the effects of multiple scattering of electrons. The limit of pressure comes from the consideration of mean free path of electrons in the medium. To ensure that the electron is not scattered twice in the scattering cell, one has to make sure that the mean free path is greater than the dimension of the scattering cell. However, in the experiment to observe appreciable reduction in the intensity of electron peak, it was necessary to go beyond the pressure limit prescribed by the mean free path considerations. Therefore, it was necessary to check for the effects due to multiple scattering. Figure (4.1) shows the graph plotted for $\ln \left[\frac{I_{e2}}{I_{e1}} \frac{I_{\lambda c1}}{I_{\lambda c2}} \right]$ versus $(P_1 - P_2)$ (see equation (3.8)) for a few electron energies in helium and neon. The target gas pressure was varied from 0 to a maximum of 2.5×10^{-2} Torr. As suggested by equation (3.8), they are straight lines and the slope represents

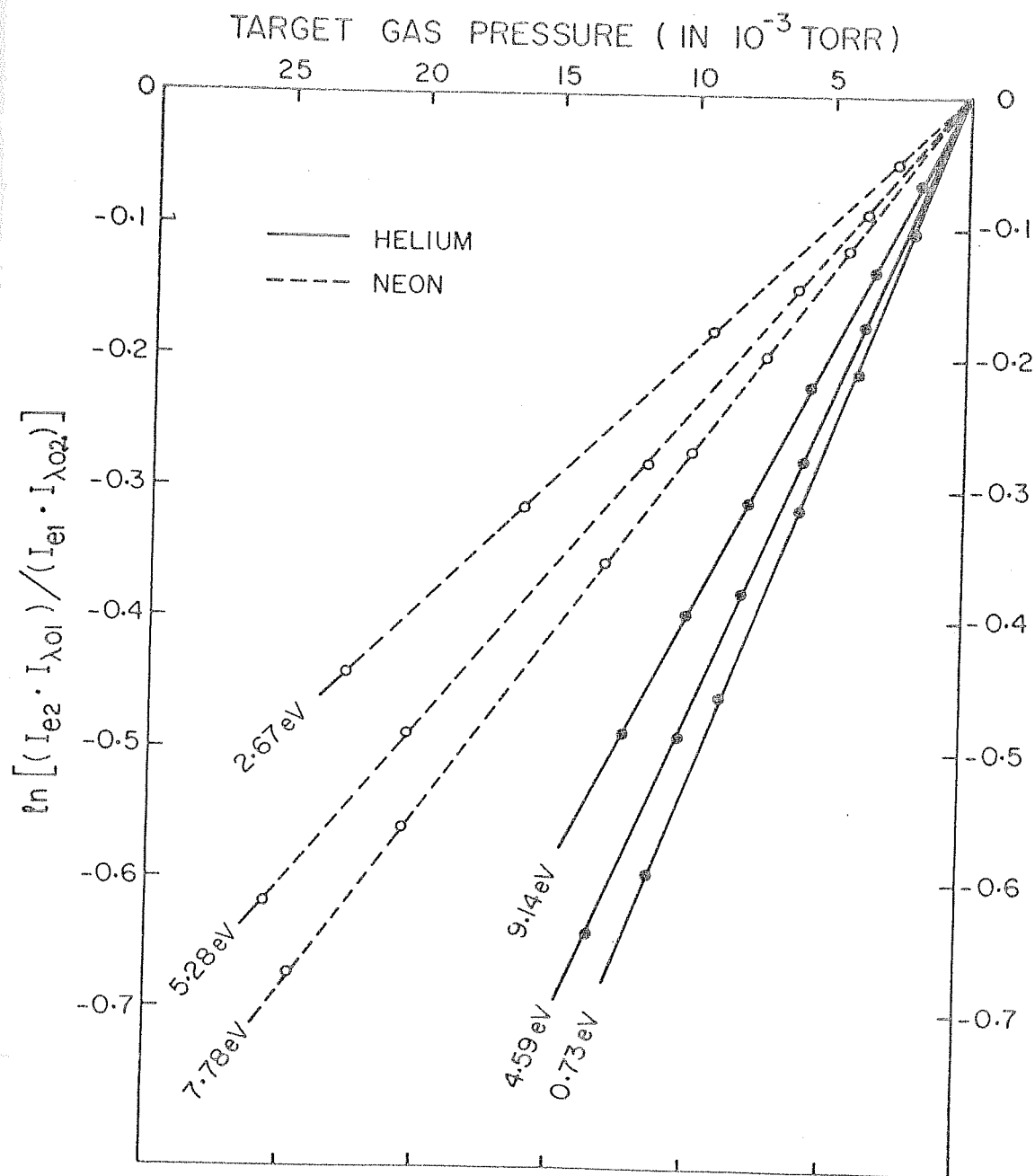


FIG. 4.1 PLOT OF $\ln \left[\frac{I_{e2} I_{\lambda 01}}{I_{e1} I_{\lambda 02}} \right]$ VERSUS $(P_1 - P_2)$ FOR HELIUM AND NEON

total scattering cross-section at that energy. If multiple scattering were to happen, the points, especially at higher pressure side, would tend to deviate from the straight line. Therefore, these plots suggest that the errors due to multiple scattering were negligible.

4.7 Scattering in the accelerating region

The electron scattering was also present in the accelerating region. The magnitude of scattering in this region was compared with scattering in ionising region by comparing the "effective path length" (the product of pressure and physical path length) in these region. For a target gas pressure of 2.5×10^{-2} Torr in the ionising region the pressure measured immediately after the exit slit of the ionising region was about 2×10^{-3} Torr, and in the analysing region pressure was about 8×10^{-5} Torr. Because of surge of gas through the slit, the measured pressure of 2×10^{-3} Torr is much higher than the average pressure along the electron path in the accelerating region. This is because pumping through the slits of the inner cylinder of the CMA assists differential pumping in the said region, over and above the differential pumping through the accelerating region. It is expected that the average pressure from the exit slit to the slit on the CMA is slightly greater than 10^{-4} Torr. A comparison of effective path lengths showed that the errors because of scattering in this region amounted to $\pm 0.6\%$.

4.8 Gas impurity

The gases helium, neon, krypton and xenon were obtained from British Oxygen Company and argon from Indian Oxygen Ltd. The purity specified by the manufacturers was 99.95%. Care was taken to maintain the purity of gases. The gas handling system was completely made of metal, and was evacuated before the experiment. Further purification was done by passing the gas through a cold trap before introducing to the system. A liquid nitrogen trap was used in the case of helium and neon, whereas argon, krypton and xenon were passed through a trap cooled by alcohol-acetone liquid nitrogen slurry (temperature -80°C). Therefore, the error due to the sample gas impurity was negligible.

4.9 Scattering due to ions

Photoionisation of gases results in the generation of positive ions. As the electron scattering cross-sections are generally higher (10 to 100 times) for ions than neutrals, this can introduce error in the measured cross-section. An estimation for positive ion number density was done from the intensity of photon flux incident on the source gas, the number density of target particles in the ionising region and the photoionisation cross-section at different photon energies. It was assumed that ions were again converted to neutrals after the collision with the walls of the

Table 4.1

Table of all contributing errors in the experiment
for the measurement of scattering cross-section.

1. Pressure measurement	: $\pm 0.15\%$
2. Thermal transpiration	: $\pm 0.4\%$
3. Uncertainty in scattering path length	: $\pm 2.1\%$
4. Counting statistics	: $\pm 1.5\%$
5. Forward scattering	: $\pm 0.5\%$
6. Scattering in the accelerating region	: $\pm 0.6\%$

Coherent sum : $\pm 5.3\%$

Incoherent sum : $\pm 2.7\%$

ionisation chamber. Thus the life time of ion was the time taken by them to reach the walls. By this method, the ratio of ionic species in equilibrium with the neutrals, to the neutral species could be determined. This ratio was found to be very small, of the order of 10^{-4} to 10^{-5} . Since the fraction is very low, the error arising because of scattering due to ions could be safely neglected.

4.10 Uncertainty in incident electron energy

Photoelectrons are produced by photoionisation of noble gas atoms by VUV resonance lines, and their energies could be fixed with high degree of accuracy. Because of this, the uncertainty in fixing the electron energy is almost negligible.

The coherent sum of all the contributing errors discussed above was $\pm 5.3\%$ and it acted as the upper limit estimate of the actual error in the experiment. The incoherent sum (square root of sum of squares) of all these errors was found to be $\pm 2.7\%$ and it represented most probable error in the experiment. All the errors discussed above are given in table 4.1.

CHAPTER FIVE

RESULTS AND DISCUSSION

The electron scattering cross-sections for noble gases have been measured at seventeen electron energies ranging from 0.7 to 10 eV using a photoelectron source. In the case of helium and neon, source gas was always different from the target gas and equation (3.8) was used to calculate scattering cross-sections. For cross-section measurements in the case of argon, krypton and xenon source and target gases were different in some cases, and were same in the other. Both equations (3.8) and (3.11) were used to compute the scattering cross-section, wherever applicable.

The variation of amplitudes of photoelectron peaks could be demonstrated by the semilogarithmic plots for

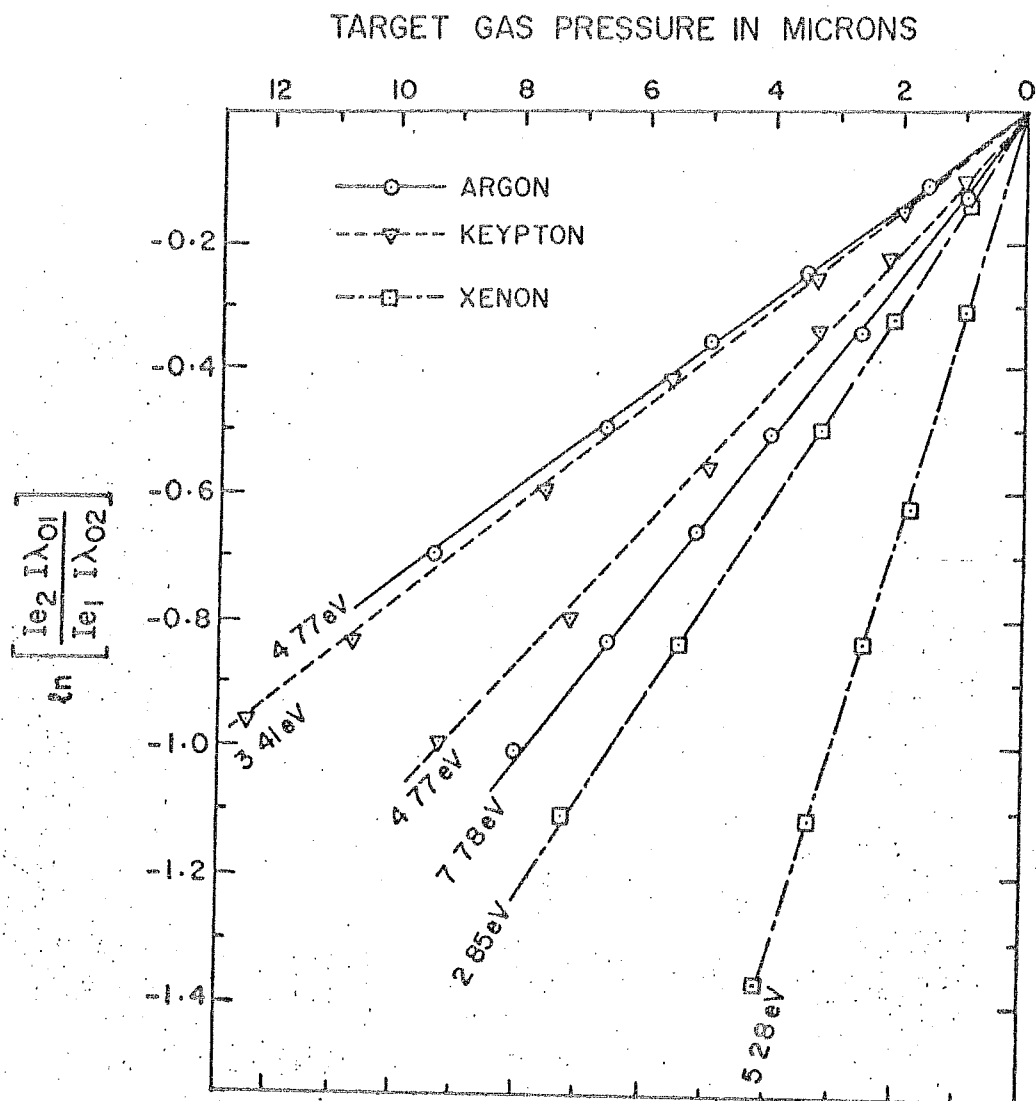


Fig. 5-1 PLOT OF $\ln \left[\frac{I_{e2} I_{\lambda 01}}{I_{e1} I_{\lambda 02}} \right]$ VERSUS
 $(P_1 - P_2)$ FOR Ar, Kr AND Xe FOR
 FEW SELECTED ENERGIES.

$\ln \left[\frac{I_{e2} I_{\lambda 01}}{I_{e1} I_{\lambda 02}} \right]$ (for source gas different from target gas) or $\ln \left[\frac{I_{e2} I_{\lambda 01} \rho_1}{I_{e1} I_{\lambda 02} \rho_2} \right]$ (for target and source gas same) against $(P_1 - P_2)$ of equation (3.8) or (3.11). Such plots in the case of helium and neon have already been shown in previous chapter (Figure 4.1). Similar semilogarithmic plots in the case of argon, krypton and xenon at a couple of representative energies are shown in Figure 5.1.

In this chapter, results obtained for electron scattering cross-sections of noble gases would be presented and discussed in detail. The results as obtained in the present work would also be compared with those reported from other experiments as well as from recent theoretical calculations.

5.1 Helium

The total electron-helium scattering cross-sections as measured in the present experiment are shown in Figure 5.2, for seventeen electron energies ranging from 0.7 to 10 eV. The results of the present experiment are shown along with those reported by Nesbet [1979], Stein et al [1978], Kennerly and Bonham [1978] and Nickel et al [1985]. Error bars at only three energy points have been shown, so as to give a fair idea about the accuracy of the experiment at different electron energies. Nickel et al [1985], using transmission technique, have made scattering cross-section measurements at five energies only between 4 and 10 eV. Their reported

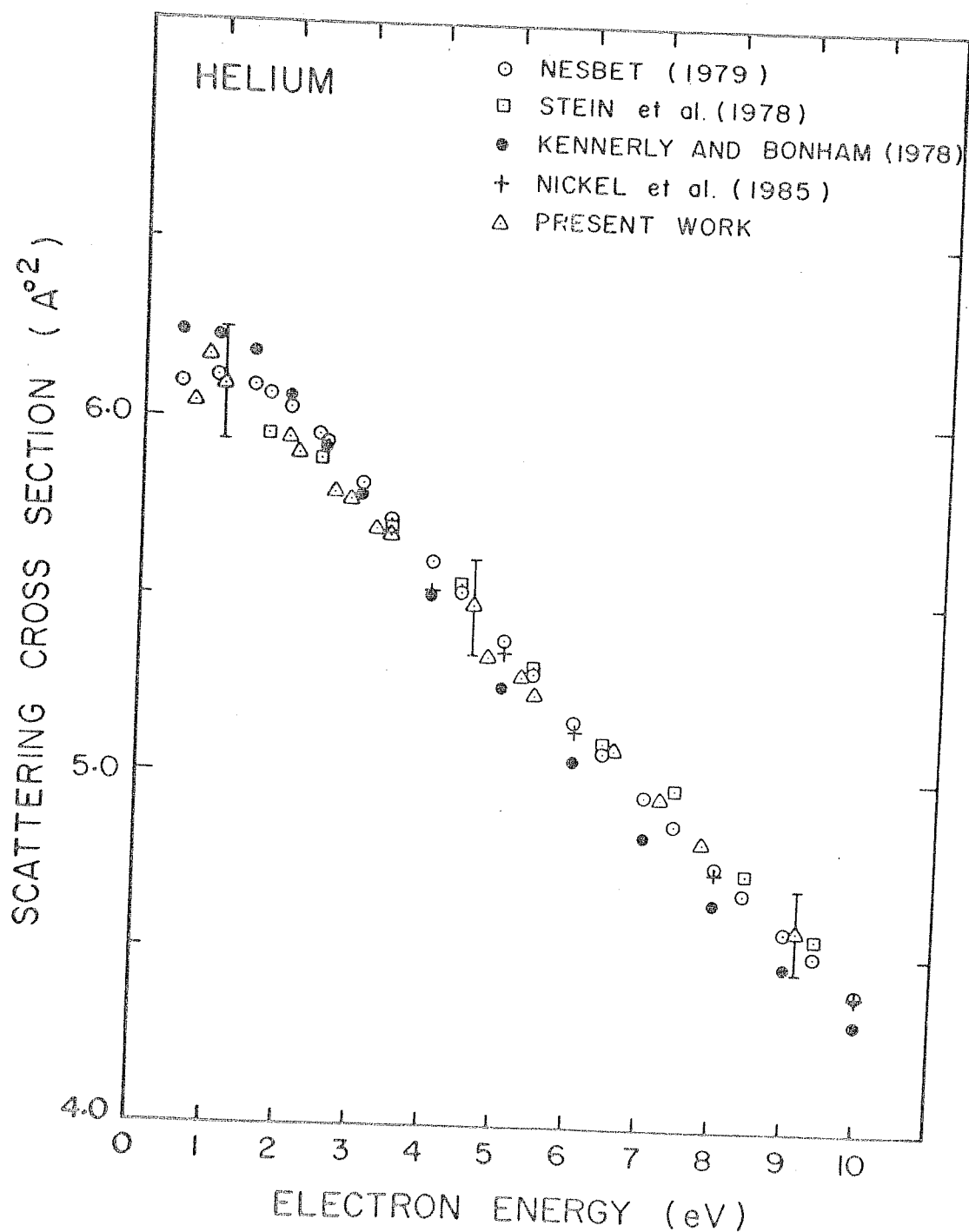


FIG.5.2 ELECTRON-HELIUM SCATTERING CROSS SECTION
AS A FUNCTION OF ELECTRON ENERGY
BELOW 10 eV

values of scattering cross-section agree favourably with the results reported in the present experiment. Kennerly and Bonham [1978], using time-of-flight technique have reported data at thirteen energy points between 0.5 and 10 eV, with an estimated error of $\pm 3\%$. Their measured values below 2.5 eV are higher than those reported in the present work while at electron energies larger than 4 eV, their cross-sections are smaller. Using transmission technique, Stein et al [1978] have measured electron-helium scattering cross-sections at ten energy points between 1.5 and 9 eV. The results obtained by Stein et al are comparable with the results reported in the present work, in this energy region. Andrick and Bitsch [1975] have computed total electron-helium scattering cross-sections between 2 to 19 eV by experimental investigation of differential cross-section, and subsequent phase shift analysis. The values reported by them also compare well with the results reported in the present work. However, these values have not been shown in the figure for lack of space. Also shown in the figure 5.2 are the results of variational calculations by Nesbet [1979] at a large number of points between 0.5 and 10 eV. These are very accurate computations obtained using variational principle to calculate S and P-wave shifts and taking into account dipole and quadrupole polarisabilities. These calculations are accurate to within the quoted error limit of $\pm 1\%$ and these are considered as the best known so far. Results of the present experiment match favourably well with the values reported by Nesbet. The scattering cross-sections as

Table 5.1

Total electron-helium scattering cross-sections
A comparison of results obtained in the present
work with those reported by Nesbet[1979].

Electron Energy (eV)	Electron Scattering Cross-sections in \AA^2		Difference %
	Present work	Nesbet (1979)	
0.73	6.04	6.105	- 1.06
0.91	6.16	6.115	+ 0.74
1.09	6.09	6.110	- 0.33
2.00	5.94	6.027	- 1.44
2.18	5.90	5.985	- 1.42
2.67	5.79	5.890	- 1.70
2.85	5.77	5.855	- 1.45
3.23	5.69	5.770	- 1.39
3.41	5.68	5.735	- 0.96
4.59	5.48	5.465	+ 0.27
4.77	5.33	5.430	- 1.84
5.28	5.28	5.310	- 0.56
5.46	5.23	5.275	- 0.85
6.55	5.08	5.040	+ 0.79
7.22	4.94	4.895	+ 0.92
7.78	4.81	4.785	+ 0.52
9.14	4.57	4.540	+ 0.66

measured in the present experiment at seventeen electron energies are summarised in table 5.1 alongwith the results of Nesbet [1979] and the percentage differences between the two cases has been tabulated as a function of the electron energy. The difference in the two cases varies from +0.9 to -1.8 percent, which is well within the stipulated error bars.

5.2 Neon

The total electron-neon scattering cross-sections were measured at seventeen electron energies below 10 eV, and the results are presented in figure 5.3 alongwith measured and computed cross-sections by other investigators [Stein et al, 1978; O'Malley and Crompton, 1980; Nickel et al 1985, and McEachran and Stauffer 1985]. Nickel et al have reported cross-sections at only five energy points between 4 and 10 eV, while Stein et al have reported only four values between 3 and 10 eV. McEachran and Stauffer [1978, 1984, 1985] have used the method of polarised orbitals using adiabatic exchange approximation, with the polarisation potential scaled to the correct asymptotic form. They have reported values at six points between 0.5 and 10 eV, and the reported values agree very well with the values measured in the present work. O'Malley and Crompton [1980] have derived the total scattering cross-sections measured by them using Modified Effective Range Theory (MERT). They have reported cross-sections only below 2.3 eV. Other measurements are due to Salop and Nakano [1970] and Kauppila et al [1981], both

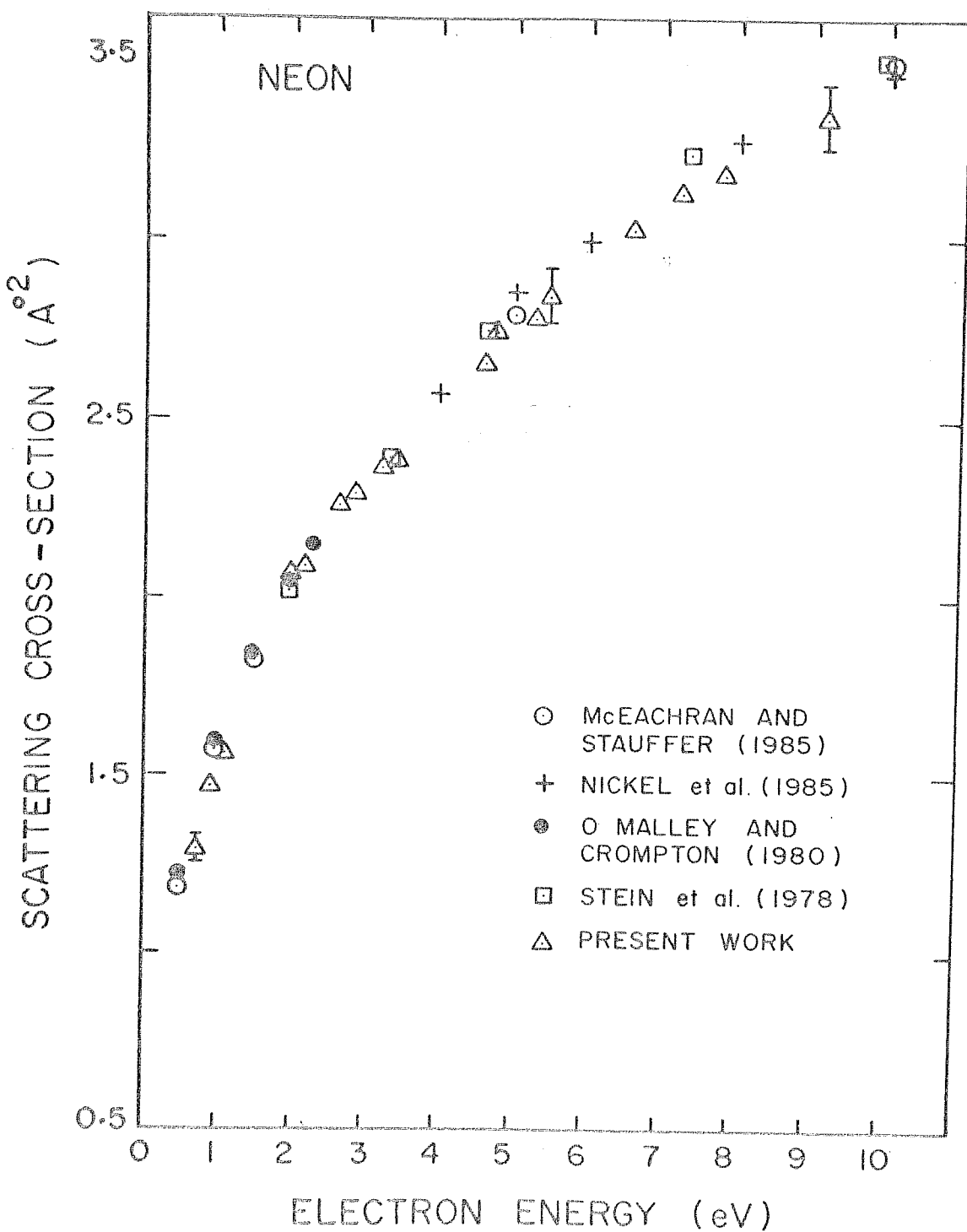


FIG. 5.3 ELECTRON-NEON SCATTERING CROSS SECTION
AS A FUNCTION OF ELECTRON ENERGY BELOW 10 eV

Table 5.2. Total electron scattering cross-sections for neon as measured in the present experiment.

Electron energy (eV)	Electron Scattering Cross-sections(\AA^2)
0.73	1.29
0.91	1.47
1.09	1.56
2.00	2.05
2.18	2.09
2.66	2.26
2.85	2.28
3.23	2.36
3.41	2.38
4.59	2.65
4.77	2.74
5.28	2.80
5.46	2.84
6.55	3.02
7.22	3.12
7.78	3.17
9.14	3.33

being transmission techniques. Dasgupta and Bhatia [1984] have computed cross-sections using the method of polarised orbitals. The above results are in good agreement with the values reported in the present work in the energy region between 0.7 to 10 eV. Fon and Berrington [1981] using R-matrix calculations reported cross-sections at only two energies at 5 and 10 eV respectively, and their values also compare well with those reported by other investigators. In general, there is a good agreement in the values for cross-sections for neon in the low energy region. The scattering cross-sections are measured in the present experiment are given in table 5.2. It may be pointed out here that the cross-sections reported by Salop and Nakano [1970], Kauppila et al [1981], Dasgupta and Bhatia [1984] and Fon and Berrington [1981] have not been included in figure 5.3 so as to avoid any possible overcrowding of data points at different electron energies.

5.3 Argon

The total electron-argon scattering cross-sections measured in the present experiment are shown in figure 5.4 at electron energies ranging from 0.7 to 10 eV, along with error bars shown at two representative energies only. Also shown in the figure are the measured cross-sections reported by Jost et al [1983], Nickel et al [1985], Ferch et al [1985a] and Charlton et al [1980] and theoretically computed values by Fon et al [1983], Dasgupta and Bhatia

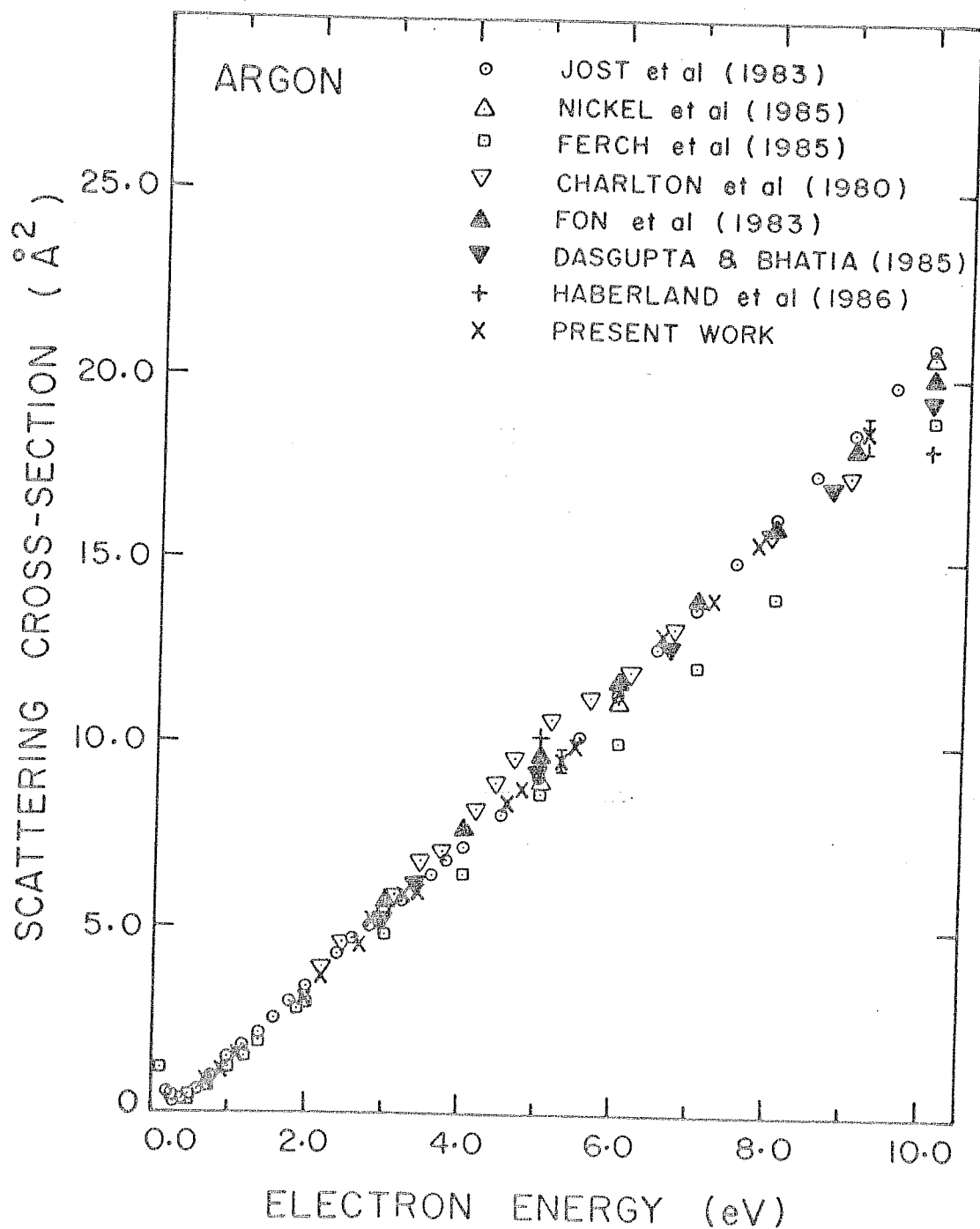


FIG.5.4 ELECTRON-ARGON SCATTERING CROSS SECTION
AS A FUNCTION OF ELECTRON ENERGY
BELOW 10 eV

[1985] and Haberland et al [1986]. However, cross-sections obtained by Kauppila et al [1986, 1977] have not been included in the figure for lack of space. Also, the results reported by Bell et al [1984], McEachran and Stauffer [1983] and Yau et al [1978, 1980] could not be shown in figure 5.4. The cross-sections obtained by McEachran and Stauffer [1983] (treating adiabatic approximation only) are higher by about 6 to 35% at 3 to 10 eV respectively as compared to the results obtained in the present experiment. Yau et al [1980] also computed electron-argon cross-sections using frozen core method and perturbed core method [Yau et al, 1978]. The results agree quite well with those reported in the present work upto 5 eV, but at higher electron energies there is a discrepancy, as high as 35% at 10 eV. Bell et al [1984] and Fon et al have computed the cross-sections using R-matrix theory and the values reported by them are very close to each other. For this reason, the cross-section data of Fon et al only has been retained for further discussion.

The scattering cross-sections for argon as measured by Nickel et al [1985] have been reported at five energies between 4 and 10 eV. However, cross-sections at only three representative energies have been shown in Figure 5.4. The values of cross-sections by Nickel et al and Jost et al [1983] reported at large number of energy points are comparable to the results obtained in the present experiment within the stipulated experimental error. The cross-sections measured by Charlton et al [1980] using

Table 5.3. Total electron scattering cross-sections for argon as measured in the present work.

Electron energy (eV)	Electron Scattering Cross-sections(\AA^2)
0.73	0.96
0.91	1.20
1.09	1.54
2.00	3.09
2.18	3.66
2.66	4.60
2.85	5.23
3.23	5.90
3.41	6.04
4.59	8.41
4.77	8.81
5.28	9.58
5.46	9.96
6.55	12.93
7.22	13.90
7.78	15.41
9.14	18.45

time-of-flight technique in the energy range between 2 and 10 eV are in good agreement with our results in the energy ranges from 2 to 3.5 and from 6.5 to 9 eV. However, in the energy region between 3.5 to 6.5 eV, the cross-sections reported by Charlton et al are higher to a maximum of 12% at 5 eV. Upto 5 eV, the measured cross-sections by Ferch et al [1985a] are in good agreement with our results, but above 5 eV, the results reported by them are lower to the extent of 10 and 15% at 6 and 8 eV respectively. The theoretically computed cross-sections using R-matrix theory [Fon et al, 1983] and polarised orbital method [Dasgupta and Bhatia, 1985] at electron energies 3 to 10 eV match extremely well with the measured values in the present work. Haberland et al [1986], using Kohn-Sham type one particle potential model have calculated cross-sections for argon at two points below 10 eV. The cross-sections computed at 5 eV matches quite well with that obtained in the present work, while the cross-section at 10 eV is quite low.

The values of scattering cross-sections for argon as measured in the present work are given in table 5.3.

5.4 Krypton

The total electron scattering cross-sections for krypton as measured in the present experiment are shown in figure 5.5 for electron energies ranging from 0.7 to 10 eV. The results of the present experiment are shown along with

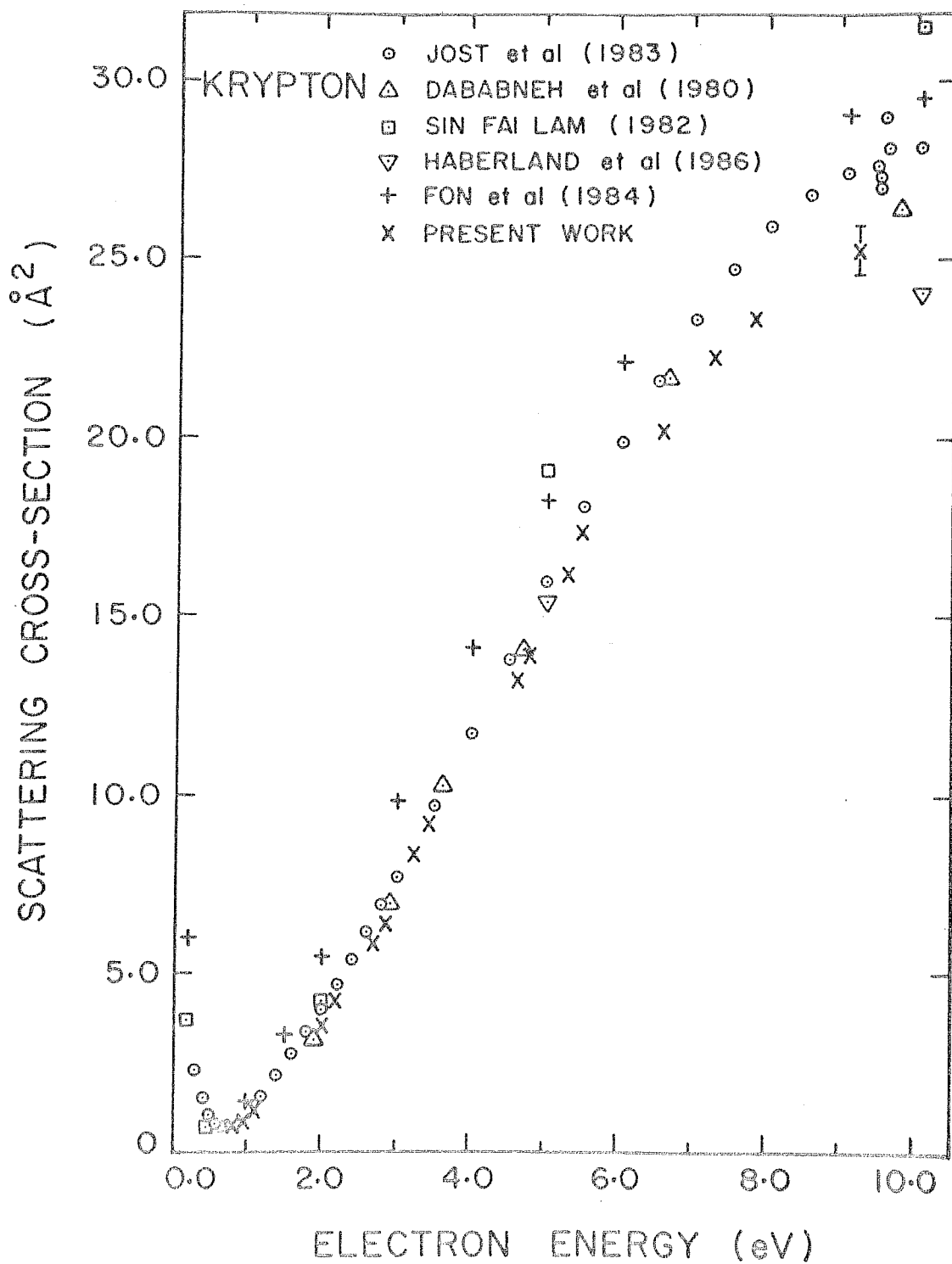


FIG.5.5 ELECTRON-KRYPTON SCATTERING CROSS SECTION
AS A FUNCTION OF ELECTRON ENERGY
BELOW 10 eV

the values of the measured cross-sections reported by Dababneh et al [1980] and Jost et al [1983] and theoretically computed results by Sin Fai Lam [1982], Fon et al [1984] and Haberland et al [1986]. Sin Fai Lam has computed the cross-sections taking into account direct and indirect relativistic effects of core electron motions as well as the polarisation effects. In figure 5.5 we have not included the results computed by McEachran and Stauffer [1984], treating exchange exactly and including only dipole part of the polarisation potential. These values are much higher than the values reported in the present work, with a difference of about 15 and 40% at 2 and 10 eV respectively. Using time-of-flight spectroscopy Gus'kov et al [1978] have measured Ramsauer-Townsend maximum for krypton below 2 eV. In the present experiment, the energy range was not suitable to investigate Ramsauer-Townsend minima in noble gases, therefore a direct comparison with the reported values by Gus'kov et al seemed to be difficult.

The total electron-krypton scattering cross-sections obtained in the present experiment are in excellent agreement with cross-sections measured by Jost et al [1983] and Dababneh et al [1980] in the energy region upto 5 eV. The values of cross-sections measured in the present work are lower by 6 to 11% at electron energies between 6 and 10 eV as compared to those reported by Jost et al and by 5 to 4% as compared to values measured by Dababneh et al. The agreement between the measured results in the present work

Table 5.4. Total electron scattering cross-sections for krypton as measured in the present work.

Electron energy (eV)	Electron Scattering Cross-sections(\AA^2)
0.73	0.74
0.91	0.90
1.09	1.19
2.00	3.54
2.18	4.17
2.66	5.79
2.85	6.36
3.23	8.33
3.41	9.14
4.59	13.10
4.77	13.84
5.28	16.12
5.46	17.31
6.55	20.17
7.22	22.20
7.78	23.29
9.14	25.20

and theoretically computed values by Sin Fai Lam is reasonably good upto 2 eV, but at higher energies, the cross-sections computed by Sin Fai Lam are very large. The theoretical computations by Haberland et al [1986] have been made only at 5 and 10 eV using one particle potential model. The cross-section at 5 eV agree very well, but at 10 eV, the computed cross-section is much less than the values reported in the present work. Results of R-matrix calculations by Fon et al [1984] indicate that the shape of the cross-section curve reported by them is similar to that obtained in the present work. But, the values of cross-sections reported by them are systematically large by more than 30 to 18% at energies between 1 to 10 eV, as compared to those obtained in the present work.

The values of cross-sections reported in the present work for krypton are given in table 5.4.

5.5 Xenon

The total electron scattering cross-sections for xenon measured in the present experiment are shown in figure 5.6 for electron energies ranging from 0.7 to 10 eV. The results of the present work are shown along with the measured cross-sections reported by Jost et al [1983, 1984], Dababneh et al [1980] and Nickel et al [1985] and theoretically computed cross-sections by Sin Fai Lam [1982] and Haberland et al [1986]. The previously measured cross-sections by Jost et al [1983] were later on revised by them [Jost et al,

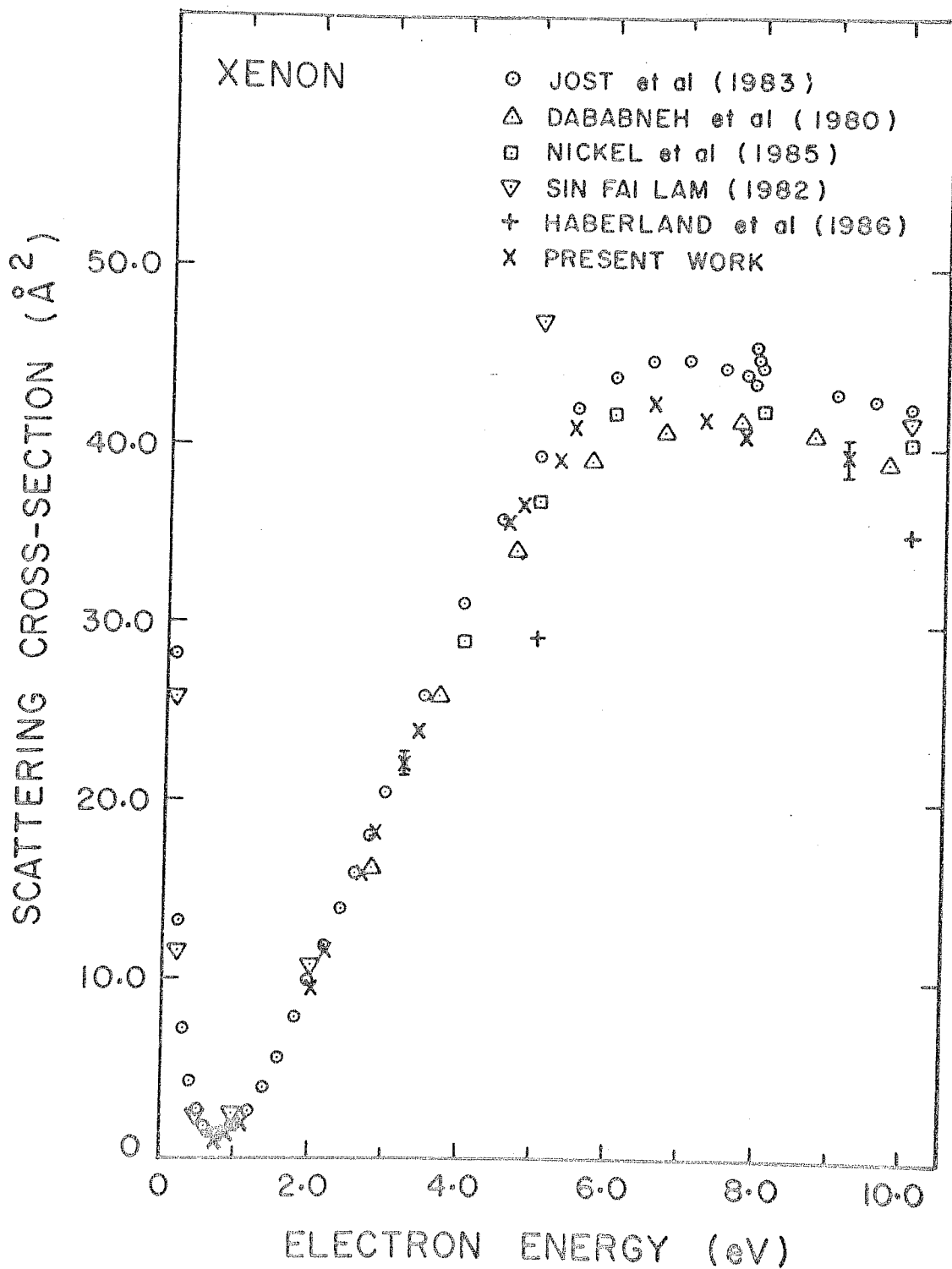


FIG.5.6 ELECTRON-XENON SCATTERING CROSS SECTION
AS A FUNCTION OF ELECTRON ENERGY
BELOW 10 eV

1984] and only the revised values of cross-sections have been included in figure 5.6. As in the case of krypton, Gus'kov et al [1978] have made measurement only below 2 eV, and the results are not shown in Figure 5.6, because the energy range for comparison is too small. Similarly, cross-sections calculated by McEachran and Stauffer [1984] have also not been shown in the figure, as the reported cross-sections are much larger than the measured values obtained in the present experiment.

Nickel et al [1985] have made cross-section measurement only at five energies between 5 and 10 eV, whereas there are eight values of cross-sections measured by Dababneh et al at electron energies from 2.8 to 10 eV. Jost et al [1984] have reported large number of data points in a wide range of energy. The scattering cross-sections obtained in the present work are in fairly good agreement with those reported by Nickel et al and Dababneh et al throughout the energy region varying from 0.7 to 10 eV, except for a small region between 5.5 and 7.5 eV, where the cross-section values reported by Dababneh et al are smaller. There is an excellent agreement between the cross-section values reported by Jost et al [1984] for electron energies less than 5.5 eV, but at higher energies the values reported by Jost et al are higher by 6 to 9% at energies between 6.5 and 9.5 eV. The theoretically computed cross-sections by Sin Fai Lam [1982] compare well with those reported in the present work only upto 2 eV, but at higher energies the

Table 5.5. Total electron scattering cross-sections for xenon as measured in the present experiment.

Electron energy (eV)	Electron Scattering Cross-sections(\AA^2)
0.73	1.10
0.91	1.28
1.09	1.90
2.00	9.58
2.18	11.69
2.66	16.01
2.85	18.28
3.23	22.13
3.41	23.91
4.59	35.57
4.77	36.47
5.28	39.09
5.46	40.86
6.55	42.33
7.22	41.38
7.78	40.54
9.14	39.27

values differ by a large amount. As in krypton, Haberland et al [1986] have reported cross-sections only at 5 eV and 10 eV, but the values for cross-section lie very much below the values obtained in the present work. There is in general, a large discrepancy between the results reported by theoretical computations and experimental techniques.

The values of scattering cross-sections for xenon at seventeen electron energies ranging from 0.7 to 10 eV are being given in table 5.5.

CHAPTER SIX

CONCLUSION AND SCOPE FOR FUTURE WORK

6.1. Conclusion

From the results discussed in chapter 5, it is evident that the values of scattering cross-section for helium and neon, as measured in the present experiment compare well with those reported from other measurements and theoretical calculations. However, not much work has been done to measure the electron scattering cross-sections for these gases at electron energies below 2 eV. In the case of helium the only recent measurements reported are by Gus'kov et al [1978], Kennerly and Bonham and by the authors of the present work. In the case of neon also, only a few recent measurements for the scattering cross-sections have been carried out at

electron energies less than 2 eV. These include the investigations by Gus'kov et al [1978], Salop and Nakano [1970], O'Malley and Crompton [1980] and by the authors of the present work. In the light of this argument, it is clear that more measurements of electron scattering cross-sections for helium and neon are required in the electron energy region below 2 eV.

A different picture emerges in the case of argon, krypton and xenon. Except in the case of argon, the agreement in the values of scattering cross-sections as given by different theoretical calculations and measurements is, in general, not as good as it was in the case of helium and neon. In the case of argon, the computations by R-matrix method and polarised orbital method used by Fon et al [1983] and Dasgupta and Bhatia [1985] could faithfully reproduce the measured values of cross-sections in the electron energy region below 10 eV. The situation in the case of krypton and xenon is somewhat different. Firstly, not enough work has been done to compute the scattering cross-sections at low energies. Secondly, from whatever little is available from literature, it appears that the theoretical values of cross-sections computed by one method do not seem to agree with those computed by other methods. Also, there is, in general no agreement between the cross-sections reported both by experimental methods and theoretical techniques. In view of this, it is stressed that more theoretical work needs to be carried out in this

direction.

From the results discussed in the last chapter, it is clear that the values of electron scattering cross-sections for noble atoms as measured in the present experiment may be the best as compared to those reported by other investigators. Firstly, the accuracy of the measurement of $\pm 2.7\%$ as estimated in the present experiment is definitely better than that reported by many other investigators. Secondly, the number of energy points at which cross-sections have been measured in the present work, is much larger than that reported in a few other experiments. It may be pointed out here that at low electron energies, the photoelectron source is better than the conventional electron gun source in at least two respects; the energy of the photoelectron peak is defined with larger accuracy and the energy spread of the peak (FWHM) is much smaller.

6.2. Scope for future work

The present experimental set up can be used without any modification, to measure electron scattering cross-sections for noble gases at very low electron energies, say below 1 eV. At very low energies, this method may be preferred to other conventional methods because of the reasons discussed in chapter 1. In the case of helium and neon, measurement of scattering cross-sections (below 1 eV) at a large number of points would help to establish the scattering length

precisely. The scattering length is obtained by extrapolating the scattering cross-section to zero energy axis. Scattering length is of interest, since it represents zero energy scattering phenomena. The most accurate evaluation of scattering length for helium has been computed by Nesbet [1979] with an estimated accuracy of +0.5%.

For argon, krypton and xenon, the measurement of scattering cross-sections at larger number of energy points below 1 eV would help to determine the Ramsauer-Townsend minima accurately. Different experiments carried out so far have established that the minima occurred between 0.5 and 0.9 eV for noble gases, but further investigations are needed for the precise determination of locations as well as for the measurement of value of cross-sections at the minima. It would be interesting to measure the scattering length for these noble atoms also.

To undertake such an experiment, one should have a powerful VUV light source with a larger number of wavelengths available in the desired energy region. A synchrotron radiation source is the ideal one capable of providing VUV continuum. However, in the absence of continuum VUV sources, many-lined source, emitting a very large number of closely spaced emission lines would be a good substitute. A thyratron-triggered sliding spark discharge lamp is available in our laboratory. This provides a large number of

VUV lines corresponding to emission from multi-ionised gas atoms used inside the light source. Since there are a large number of closely lying emission lines, a VUV monochromator has to be used with this light source.

The scattering study of some molecular gases is also extremely interesting. Recently, some of the molecular gases, for example methane [Ferch et al, 1985b] have been identified to be exhibiting Ramsauer-Townsend phenomena. On the other hand, low energy scattering cross-section data for O_2 , N_2 etc. are very much required to model cooling of electron gas in the earth's ionosphere as well as to estimate the heat budget of the upper atmosphere. Also there are a few molecular gases, whose cross-section data at low electron energies are of much importance to the branch of gaseous dielectrics and laser physics. The cross-section data of N_2 is particularly important to collision physicists because of the resonances obtained in the cross-sections at electron energies between 1.8 and 3.6 eV [Chandra and Temkin, 1976]. These resonances have been studied experimentally by Golden [1966] and Jost et al [1983]. In addition to this, a weak resonance below 1.8 eV, not predicted by theory, was also obtained by Golden but has not been identified by Jost et al. There is a controversy about this weak resonance in molecular nitrogen. This structure may be spurious as suggested by some. Another suggestion is that, it may be due to resonant superelastic collisions with vibrationally excited N_2 present in the

target gas. However, there is a lot of scope for investigating the structure in the cross-section of N_2 using the present experiment.

LIST OF PUBLICATIONS

1. Electron-helium and electron-neon scattering cross-sections at low energies using a photoelectron source
Vijay Kumar, E. Krishnakumar and K.P. Subramanian
J. Phys. B: Atom. Mol. Phy. 20 (1987) 2899-2910

2. Total electron scattering cross-sections for argon, krypton, and xenon.
K.P. Subramanian and Vijay Kumar
J. Phys. B: Atom. Mol. Phys., IN PRESS

REFERENCES

1. Aksela, S., Karras, M., Pessa, M., and Souminen, E., 1970, Rev. Sci. Instrum., **41**, 351
2. Aksela, S., 1971, Rev. Sci. Instrum., **42**, 810
3. Alger, D., Dagnall, R.M., Sylvester, M.D., and West, T.S., 1972, Anal. Chem., **44**, 2255
4. Allen, C.W., 1982, "Astrophysical Quantities", (The Athlone Press, London)
5. Allis, W.P., 1956, "Handbuch der Physik", (Springer, Berlin), Vol. 21, p. 383
6. Andrick, D., and Bitsch, A., 1975, J. Phys. B: Atom. Mole. Phys., **8**, 393
- 7. Bederson, B., and Keiffer, L.J., 1971, Rev. Mod. Phys., **43**, 601
8. Bekefi, G., (ed.), 1976, "Principles of Laser Plasmas", (Wiley Interscience, New York)
9. Bell, K.L., Scott, N.S., and Lennon, M.A., 1984, J. Phys. B: Atom. Mole. Phys., **17**, 4757
10. Berrington, K.A., Burke, P.G., Chang J.J., Chivers A.T., Robb, W.D., and Taylor, K.T., 1974, Comput. Phys. Commun., **8**, 149
11. Berrington, K.A., Burke, P.G., LeDourneuf, M., Robb, W.D., Taylor, K.T., and Lan Vo Ky, 1978, Comput. Phys. Commun., **14**, 367
12. Blaauw, H.J., de Heer, F.J., Wagenaar, R.W., and Barends, D.H., 1977, J. Phys. B: Atom. Mole. Phys., **10**, L299

13. Blaauw, H.J., Wagenarr, R.W., Barends, D.H., and de Heer F.J., 1980, J. Phys. B: Atom. Mole. Phys., **13**, 359
14. Brode, R.B., 1925, Phys. Rev., **25**, 636
15. Brunt, N.H., Read, F.H., and King, G.C., 1977, J. Phys. E: Sci. Instrum., **10**, 134
16. Burche, E., Lillienthal, O., and Schrodter, K., 1927, Ann. Physik. **84**, 279
17. Burke, P.G., and Seaton, M.J., 1971, in "Methods of Computational Physics", Eds. Alder, B., Fernbach, S., and Rotenberg, M., Vol. 10, (Academic Press, New York and London), p. 1
18. Cairns, R.B., and Samson, J.A.R., 1965, J. Geophys. Res., **70**, 99
19. Callaway, J., 1978, Phys. Rep., **45**, 89
20. Callaway, J., 1980, Advan. Phys., **29**, 771
21. Chandra, N., and Temkin, A., Phys. Rev., **A13**, 188
22. Charlton, M., Griffith, T.C., Heyland, G.R., and Twomey, T.R., 1980, J. Phys. B: Atom. Mole. Phys., **13**, L239
23. Cherrington, B.E., 1979, "Gaseous Electronics and Gas Lasers", (Pergamon, New York)
24. Christophorou, L.G., Sauers, I., James, D.R., Rodrigo, H., Pace, M.O., Carter, J.G., and Hunter, S.R., 1984, IEEE Trans. Electr. Insula., **EI-19**, No. 6, 550
25. Chriostophorou, L.G., (ed.), 1984, "Electron-Molecule Interactions and Their Applications", Vol. 2, (Academic Press Inc., Florida)

26. Cook, G.R., and Ching, B.K., (eds.), 1965, "Absorption, Photoionisation, and Fluorescence of Some Gases of Important in the Study of the Upper Atmosphere", Aerospace Corporation, Ballistic systems and Space Division, Air Force System Command, Los Angeles Air Force Station, (Los Angeles, California)
27. Crompton, R.W., Elford, M.T., and Jory, R.L., 1967, *Austra. J. Phys.*, **20**, 369
28. Dababneh, M.S., Kaupilla, W.E., Downing, J.P., Laperriere, F., Pol, V., Smart, J.H., and Stein, T.S., 1980, *Phys. Rev.*, **A22**, 1872
29. Dalba, G., Fornasini, P., Lazzizzera, I., Ranieri, G., and Zecca, A., 1979, *J. Phys. B: Atom. Mole. Phys.*, **12**, 3787
30. Dalgarno, A., 1968, in "Advances of Atomic and Molecular Physics", Vol. 4, eds. Bates, D.R., and Estermann, I. (Academic Press, New York), p. 381
31. Dasgupta, A., and Bhatia, A.K., 1984, *Phys. Rev.*, **A30**, 1241
32. Dasgupta, A., and Bhatia, A.K., 1985, *Phys. Rev.*, **A32**, 3335
33. Demkov, Yu. N., 1958, "Variational Principles in Collision Theory", (State Publishing House for Physics and Mathematics Moscow)
34. Ditchburn, R.W., 1960, *Proc. Phys. Soc. (London)*, **A75**, 461
35. Dushman, S., 1962, "Scientific Foundations of Vacuum Technique", 2nd edn., (John Wiley, New York)
36. Edmonds, T., and Hobson, J.P., 1965, *J. Vac. Sci. Technol.*, **2**, 182
37. Ferch, J., Raith, W., and Schroder, K., 1980, *J. Phys. B: Atom. Mole. Phys.*, **13**, 1481

38. Ferch, J., Granitza, B., Masche, C., and Raith, W., 1985a, J. Phys. B: Atom. Mole. Phys., **18**, 967
39. Ferch, J., Granitza, B., and Raith, W., 1985b, J. Phys. B: Atom. Mole. Phys., **18**, L445
40. Fehsenfeld, F.C., Evenson, K.M., and Broida, H.P., 1965, Rev. Sci. Instrum., **36**, 294
41. Fon, W.C., and Berrington K.A., 1981, J. Phys. B: Atom. Mole. Phys., **14**, 323
42. Fon, W.C., Berrington, K.A., Burke, P.G., and Hibbert, A., 1983, J. Phys. B: Atom. Mole. Phys., **16**, 307
43. Fon, W.C., Berington, K.A., and Hibbert, A., 1984, J. Phys. B: Atom. Mole. Phys., **17**, 3279
44. Gardner, J.L., and Samson, J.A.R., 1975, J. Ele. Spectro. Rel. Phenom. , **6**, 53
45. Gestern, J.I., and Foley, H.M., 1968, J. Opt. Soc. Amer., **58**, 933
46. Golden, D.E., and Bandel, H.W., 1965, Phys. Rev., **138**, A14
47. Golden, D.E., Bandle, H.W., and Salerno, J.A., 1966, Phys. Rev., **146**, 40
48. Golden, D.E., Phys. Rev. Lett., **17**, 847
49. Goodrich, G.W., and Wiley, W.C., 1961, Rev. Sci. Instrum., **32**, 846
50. Green, A.E.S., and Barth, C.A., 1967, J. Geophys. Res., **72**, 3975
51. Gus'kov, Yu. K., Savvov, R.V., and Slobodyanyuk, V.A., 1978, Sov. Phys.- Tech. Phys., **23**, 167

52. Guthrie, A., 1963, "Vacuum Technology", (John Wiley, New York)
53. Haberland, R., Fritzsche, L., and Noffke, J., 1986, Phys. Rev., A33, 2305
54. Heddle, D.W.O., 1971, J. Phys. E: Sci. Instrum., 4, 589
55. Hudson, R.D., and Carter, V.L., 1968, J. Opt. Soc. Amer., 58, 227
56. Hudson, R.D., and Kieffer, L.J., 1970, "Bibliography of Photoabsorption Cross-section Data", JILA Information Centre Report, Joint Institute for Laboratory Astrophysics, Boulder, Colorado
57. Huxley, L.G.H., and Crompton, R.W., 1962, in "Atomic and Molecular Processes", ed. Bates, D.R., (Academic Press, New York), p. 335
58. Jones, R.K., and Bonham, R.A., 1982, Aust. J. Phys., 35, 559
59. Jones, R.K., 1985, Phys. Rev., A31, 2898
60. Jost, K., Bisling, P.G., Eschen, F., Felsmann, M., and Walther, L., 1983, Proceedings of 13th International Conference on Physics of Electron Atom Collisions, Berlin, ed. Eichler, J., (North-Holland, Amsterdam), p. 91
61. Jost, K., 1984, Unpublished and private communication
62. Kaupilla, W.E., Stein, T.S., Jesion, G., Dababneh, M.S., and Pol, V., 1977, Rev. Sci Instrum., 48, 822
63. Kaupilla, W.E., Stein, T.S., Smart, J.H., Dababneh, M.S., Ho, Y.K., Downing, J.P., and Pol, V., 1981, Phys. Rev., A24, 725
64. Kennerly, R.E., and Bonham, R.A., 1976, Chem. Phys. Lett., 43, 245

65. Kennerley, R.E., and Bonham, R.A., 1978, Phys. Rev., **A17**, 1844
66. Kohn, W., 1948, Phys. Rev., **74**, 1763
67. Kumar, V., and Krishnakumar, E., 1981a, J. Ele. Spectro. Rel. Phenom., **22**, 109
68. Kumar, V., and Krishnakumar, E., 1981b, J. Ele. Spectro. Rel. Phenom., **24**, 1
69. Kuyatt, C.E., and Simpson, J.A., 1967, Rev. Sci. Instrum., **38**, 103
70. Land, J.E., and Raith, W., 1974, Phys. Rev., **A9**, 1592
71. LeDourneuf, M., and Vo Ky Lan, 1977, J. Phys. B: Atom. Mole. Phys., **10**, L35
72. Lee Po and Weissler, G.L., 1955, Phys. Rev., **99**, 540
73. Lindau, I., Helmer, J.C., and Uebbing, J., 1973, Rev. Sci. Instrum., **44**, 265
74. MacDonald, A.D., and Tetenbaum, S.J., 1978, in "Gaseous Electronics", Vol. 1, eds. Hirsh, N.M., and Oskam, H.J., (Academic Press, New York, San Fransisco and London), p. 173
75. McDaniel, E.W. and Nighan, W.L., (eds.), 1982, "Applied Atomic Collision Physics - Gas Lasers", Vol. 3, (Academic Press, New York)
76. McEachran, R.P., and Stauffer, A.D., 1978, J. Phys. B: Atom. Mole. Phys., **11**, 2907
77. McEachran, R.P., and Stauffer, A.D., 1984, J. Phys. B: Atom. Mole. Phys., **17**, 2507

78. McEachran, R.P., and Stauffer, A.D., 1985, Phys. Lett., 107A, 397
79. Metzger, P.H., and Cook, G.R., 1965, J. Opt. Soc. Amer., 55, 516
80. Moiseiwitsch, B.L., 1966, "Variational Principles", (Wiley, London and New York)
81. Nesbet, R.K., 1979, Phys. Rev., A20, 58
82. Nesbet, R.K., 1980, "Variational Methods in Electron-Atom Scattering Theory", (Plenum, New York)
83. Nickel, J.C., Imre, K., Register, D.F., and Trajmar, S., 1985, J. Phys. B: Atom. Mole. Phys., 18, 125
84. Normand, C.E., 1930, Phys. Rev., 35, 1217
85. O'Malley, T.F., and Crompton, R.W., 1980, J. Phys. B: Atom. Mole. Phys., 13, 3451
86. Osterbrock, D.E., 1974, "Astrophysics of Gaseous Nebula", (W.H. Freeman & Co., San Fransisco)
87. Phelps, A.V., 1974, in "Gaseous Electronics Some Applications", eds. McGowan, J.W., and John, P.K., (North-Holland, Amsterdam), p. 25
88. Phelps, A.V., 1979, in "Electron-Molecule Scattering", ed. Brown, S.C., (Wiley Interscience, New York), p. 81
89. Raith, W., 1976, in "Advances in Atomic and Molecular Physics", eds. Bates, D.R., and Bederson, B., Vol. 12, (Academic Press, New York and London), p. 281
90. Ramsauer, C., 1921, Ann. Physik, 64, 513
91. Ramsauer, C. and Kollath, R., 1929, Ann. Physik,

92. Register, D.F., and Trajmar, S., 1984, Phys. Rev., **A29**, 1785
93. Rhodes, C.K., (ed.), 1979, "Excimer Laser - Topics in Applied Physics", Vol. 30, (Springer, Berlin)
94. Risley, J.S., 1972, Rev. Sci. Instrum., **43**, 95
95. Roy, D. and Carrette, J.D., 1977, "Topics in Current Physics", Vol. 4, ed. Ibach, H., (Springer, Berlin), p. 13
96. Rusch, M., 1925, Physik Z., **26**, 748
97. Rustgi, O.P., 1964, J. Opt. Soc. Amer., **54**, 464
98. Salop, A., and Nakano, N.H., 1970, Phys. Rev., **A2**, 127
99. Samson, J.A.R., 1967, "Techniques in Vacuum Ultraviolet Spectroscopy", (John Wiley, New York)
100. Samson, J.A.R., 1969, J. Opt. Soc. Amer., **59**, 536
101. Samson, J.A.R., 1970, Phil. Trans. Roy. Soc. (London), **A268**, 141
102. Samson, J.A.R., and Gardner, J.L., 1977, J. Opt. Soc. Amer., **62**, 856
103. Sar-El, H.Z., 1970, Rev. Sci. Instrum., **41**, 561
104. Schwartz, C., 1961, Phys. Rev., **124**, 1468
105. Seaton, M.J., 1968, in "Advances in Atomic and Molecular Physics", Vol. 4, eds. Bates, D.R., and Estermann, I., (Academic Press, New York and London)
106. Sevier, K.D., 1972, "Low Energy Electron spectroscopy", (Wiley Interscience), p. 238

107. Sheorey, V.B., 1976, in Proceedings of the First Workshop on Atomic and Molecular Collisions, Physical Research Laboratory, Navrangpura, Ahmedabad, India, p. 5
108. Shneider, B.I., 1977, in "Electronic and Atomic Collisions Invited Papers and Progress Reports", (ICPEAC), ed. Watel, G., (North-Holland, Amsterdam), p. 257
109. Sin Fai Lam, L.T., 1982, J. Phys. B: Atom. Mole. Phys., 15, 119
110. Stein, T.S., Kaupilla, W.E., Pol, V., Smart, J.H., and Jesion, G., 1977, Phys. Rev., A17, 1600
111. Temkin, A., and Lamkin, J.C., 1961, Phys. Rev., 121, 788
112. Tennyson, J., 1986, J. Phys. B: Atom. Mole. Phys., 19, 4255
113. Townsend, J.S., and Bailey, V.A., 1921, Phil. Mag., 42, 873
114. Townsend, J.S., and Bailey, V.A., 1922a, Phil. Mag., 43, 593
115. Townsend, J.S., and Bailey, V.A., 1922b, Phil. Mag., 44, 1033
116. Townsend, J.S., and Bailey, V.A., 1923, Phil. Mag., 46, 657
117. Vorberger, T.Y., Wacławski, B.J., and Sandstorm, D.R., 1976, Rev. Sci. Instrum., 47, 501
118. Wagenaar, R.W., and de Heer, F.J., 1985, J. Phys. B: Atom. Mole. Phys., 18, 2021

119. Wagneaar, R.W., de Boer, A., VanTubergger, T., Los, J., and de Heer, F.J., 1986, J. Phys. B: Atom. Mole. Phys., 19, 3121
120. Wallace, L., and McElroy, M.B., 1966, Planetary Space Sci., 14, 677
121. Wanneberg, B., Gelius, U., and Sieghban, K., 1974, J. Phys. E: Sci. Instrum., 7, 149
122. Wigner, E.P., 1946, Phys. Rev., 70, 15
123. Wigner, E.P., and Eisenbud, L., 1947, Phys. Rev., 72, 29
124. Yau, A.W., McEachran, R.P., and Stauffer, A.D., 1978, J. Phys. B: Atom. Mole. Phys., 11, 2907
125. Yau, A.W., McEachran, R.P., and Stauffer, A.D., 1980, J. Phys. B: Atom. Mole. Phys., 13, 377